

Rate Equations and Dynamics in the Cell

FIFTEEN 15

Chapter Overview: In which dynamic trajectories of molecules are described using rate equations

Illustration to follow

Much of our discussion of the interplay of the molecules and macromolecular complexes that fill the cell, both large and small, has been founded upon the use of arguments about chemical potentials and equilibrium constants. In living cells, however, circumstances are constantly changing. Ion channels are constantly opening and closing, enzymes are constantly catalyzing biochemical transformations and the elements of the cytoskeleton are growing and shrinking. In this chapter we introduce deterministic and statistical approaches for handling these kinds of dynamical processes within cells. In particular, this chapter introduces the use of rate equations, which provide a description of the time variation of populations of different chemical species. We illustrate these ideas with special reference to the dynamics of ion channels, enzyme kinetics and cytoskeletal assembly.

“To improve is to change; to be perfect is to change often.”

Winston Churchill

15.1 BIOLOGICAL STATISTICAL DYNAMICS: A FIRST LOOK

A cell is a bustling metropolis of chemical reactions that are linked together in complex networks of reactants and products. Whether we think about the chemical reactions that make up the metabolic pathways that guarantee the energy solvency of living cells such as are shown in Figure 5.2 (p. 000) or about the synthetic pathways that construct the structural components of such cells, ultimately, all of these pathways are built up of chemical reactions. If we measure the chemical activity of living cells we see that the rates and identities of these reactions are constantly changing to reflect the dynamics of metabolism, cell division, and motility, to name a few examples. As a result, we are faced with the challenge of putting together modeling tools that are up to the task of describing the rich dynamics of cellular life.

Thus far in this part of the book we have considered the fluid dynamics of life's watery medium and the diffusive dynamics of random walks in sparse and crowded environments. To truly tackle biological dynamics, we must also consider transformations in which a molecule changes its identity rather than just its position. We begin by examining a few case studies in cellular dynamics and then derive the mathematical toolbox to address these problems quantitatively.

15.1.1 Cells as Chemical Factories

When we first considered the composition of cells in Chapter 2, we estimated the average cell contents in terms of the numbers of each of the kinds of macromolecular component. For a review, see Section 2.1.2 on p. 000. In deriving the average values we paid no attention to the biological reality that every cell and every component within it is in a constant state of material flux. As cells go about their daily business of consuming, excreting, growing, dividing, moving around, etc., their compositions are constantly changing. Even for a cell under fairly constant conditions, which is not actively changing in size, its individual constituents are constantly being synthesized and degraded in a steady-state manner. When conditions do change, living organisms rapidly adapt by altering their complement of proteins, RNAs, lipids, other macromolecules, and even small metabolites.

Examples of the variation in cells over time at the level of the genes that are expressed were shown in Figures 3.17 (p. 000) and 3.19 (p. 000). It is technically more difficult to measure changes in protein, lipid, or metabolite levels than it is to measure changes in RNA levels, but many such experiments have indeed shown that the compositions can vary to a surprising degree over a very short time. In order to quantitatively understand the nature of these changes we must be able to describe the processes by which one kind of chemical species is transformed into another. The general theme of transformation is embodied over many different time scales and size scales in living cells. Rapid transformations can include processes such as protein phosphorylation and steps in metabolic pathways catalyzed by enzymes. Slower transformations may include the construction of new large scale assemblies such as the bundles of stereocilia at the top of a hair cell during differentiation. Because cells usually contain many copies of each individual kind of molecule, it is often useful to think of transformations at a population scale as changes in concentrations. Accordingly, several of our derivations will consider rate problems as descriptions of changes in concentrations over time. At the molecular level, however, transformations also take place, though usually in a less deterministic manner. One of the main goals of the chapter will be to integrate the molecular-level and population-level views of rate equations.

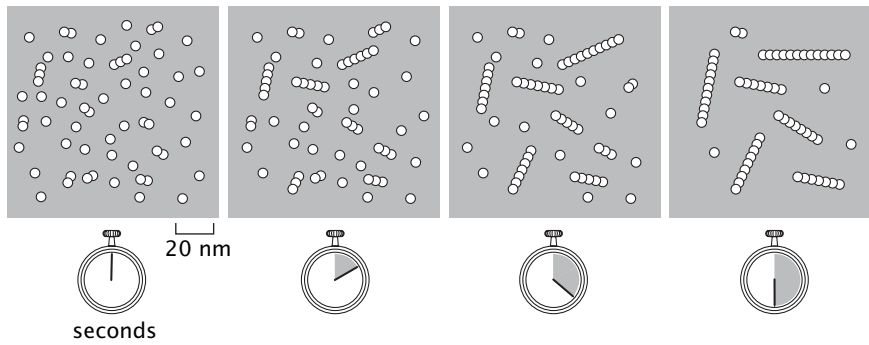
In order to give a feeling for the numbers with respect to rates of biological transformations, we consider an everyday example, literally the amount of energy that is used by the human body every day.

Estimate: Rate of ATP Synthesis in Humans To get a sense of the cellular ATP budget, consider the ATP equivalent of the average daily human diet of 2000 kcal. If we use an approximate figure of 12 kcal/mol as the energy liberated by the hydrolysis of ATP and further assume that half of the energy input in the form of our diet is turned into ATP, the number of moles of ATP synthesized each day is equal to $(1000 \text{ kcal/day}) / (12 \text{ kcal/mol}) = 80 \text{ moles/day}$. Given that the molecular weight of ATP is roughly 500 g/mol, this implies a daily turnover of more than 40 kg of ATP! Obviously a human body does not at any moment have 40 kg of ATP; this mass reflects the constant turnover accompanying metabolic processes. A total of 40 kg ATP synthesized as part of this busy metabolic enterprise.



ESTIMATE

(A) *In-vitro* polymerization



(B) *In-vivo* polymerization

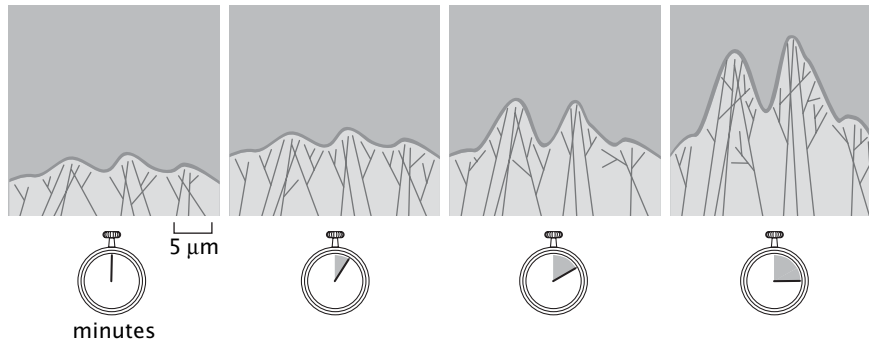


Figure 15.1 Snapshots in the life history of cytoskeletal filaments. These schematics aim to give a sense of the spatial and temporal dynamics of cytoskeletal assembly. (A) *In-vitro* assay revealing the growth of cytoskeletal filaments assembled from monomeric subunits. (B) *In-vivo* time series showing the dynamics of actin filaments growing at the leading edge of a crawling cell.

15.1.2 Dynamics of the Cytoskeleton

In addition to the constant flux of small metabolites of the cell such as ATP, there is also a surprising degree of turnover among the cell's structural elements. We have already considered the filaments of the cytoskeleton in a number of contexts, for example, as macromolecular assemblies in Chapter 2, as beams that can bend and buckle in Chapter 10, and as one of the key elements that make the cell so crowded in Chapter 14. However, we have neglected to explore the construction of these filaments and their extraordinarily dynamic nature.

All cytoskeletal polymers within living cells are constantly growing and shrinking by addition and loss of protein subunits at the same time as they are serving as construction beams and tracks for molecular motors. The rates of the process of filament assembly are illustrated in Figure 15.1 for actin filament assembly both *in vitro* and *in vivo*. *In vitro*, a solution of purified actin monomers can assemble into filaments over a time scale of a few minutes. In cells, this same kind of assembly over comparable time scales can be harnessed to push forward the leading edge of a crawling cell. The microscopic processes that attend polymerization are more complex than those shown here. For example, subunits can dissociate from the filaments as well as assemble, and in addition there are ATP hydrolysis reactions that take place within the polymer. Furthermore, the rate at which monomers are added to the growing filament depends upon the concentration of actin monomers and also on the regulatory influences of many other proteins in the cell.

The rates associated with cytoskeletal dynamics can be estimated by observing the motions of living cells. Figure 15.2 shows a fish skin cell called a keratocyte migrating on a surface. Note that actin filaments are polymerizing at the leading edge of the cell and pushing the membrane forward with the cell moving at a average rate of $0.2 \mu\text{m/s}$. Interestingly,

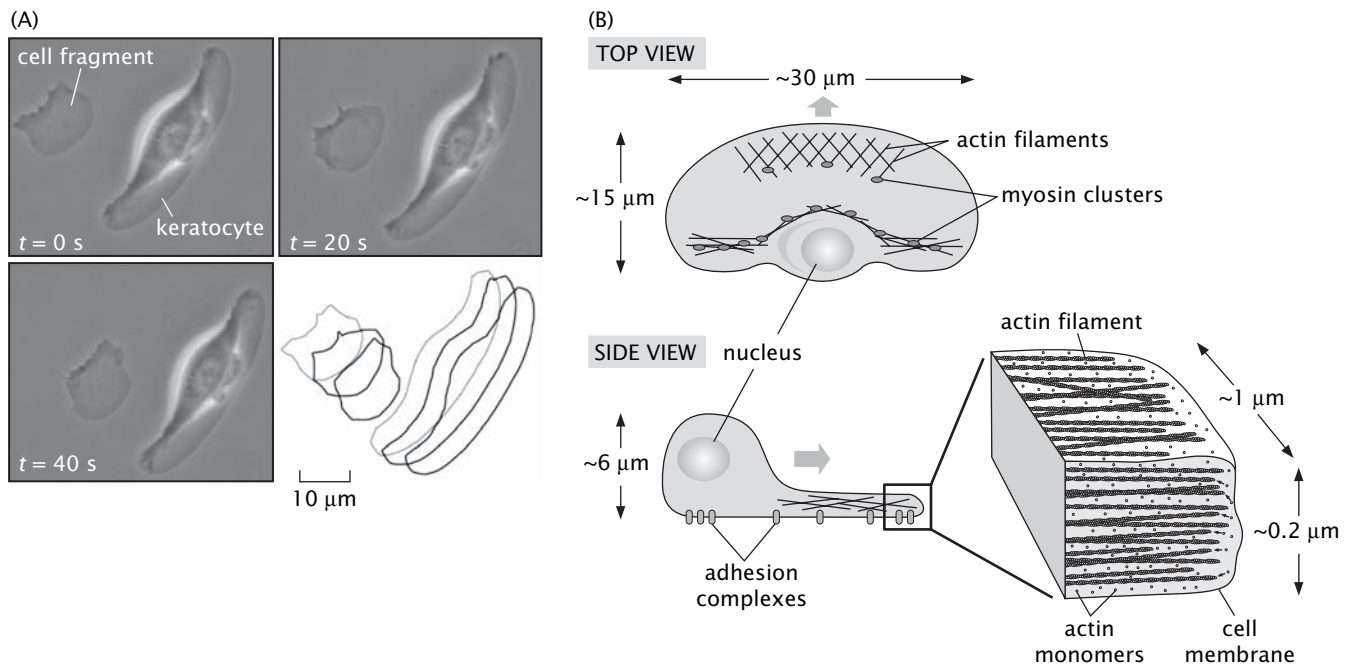


Figure 15.2 Actin-based crawling motility of epithelial cells. (A) This series of time-lapse images shows a single fish skin cell moving across a glass cover slip. Behind the cell an actin-rich fragment of another cell's lamellipodium is crawling autonomously without a nucleus or cell body. The frames were captured at 20 s intervals. The outlines show the positions of the cell and cell fragment at these time intervals. Note that they glide forward without changing shape. (B) Organization of actin filaments in the keratocyte. Seen from the top as in the microscope images, the lamellipodium is a large extension filled with a cross-linked network of actin filaments (see also Figure 14.2 on p. 000). Seen from the side, the lamellipodium is a very flat structure that drags the rounded cell body and nucleus behind it. A schematic illustration of the leading edge indicates the approximate density of actin filaments in this structure. (A, courtesy of G. Allen, K. Keren, and J. Theriot.)

this same fundamental process of orchestrated cytoskeletal assembly can be hijacked by infectious bacteria such as *Listeria monocytogenes* and used as the basis of their own motility within the cytoplasm of the infected human host cell as shown in Figure 15.3. In this case, the bacterium manipulates the host cell cytoskeletal self-assembly process to form a comet tail made up of actin filaments which pushes the bacterium along at rates ranging between 0.05 and $1.4 \mu\text{m/s}$, depending upon the host cell type. As shown in Figure 15.3(C), the key components of this system can be abstracted from their cellular context and induced to drive the motions of synthetic beads as well.

Estimate: The Rate of Actin Polymerization We can use the observed rate of cell migration in the examples considered in Figures 15.2 and 15.3 to estimate the mean rate of polymerization of actin filaments. Because the motion of both the keratocyte and *Listeria* reflect the incorporation of monomers on linear actin filaments, we can make a simple estimate of the rate of polymerization through a knowledge of the speed of the cell and the size of the individual monomers that make up the actin filament. The mean velocity of a *Listeria* bacterium in a typical epithelial host cell is comparable to the speed of keratocyte migration, about $0.2 \mu\text{m/s}$. For each G-actin subunit added to the growing filament, it increases in length by approximately 3 nm (see Figure 10.28 on p. 000). If we assume that there is a perfect linear relation between the growth of individual filaments and the macroscopic motion of the cell



ESTIMATE

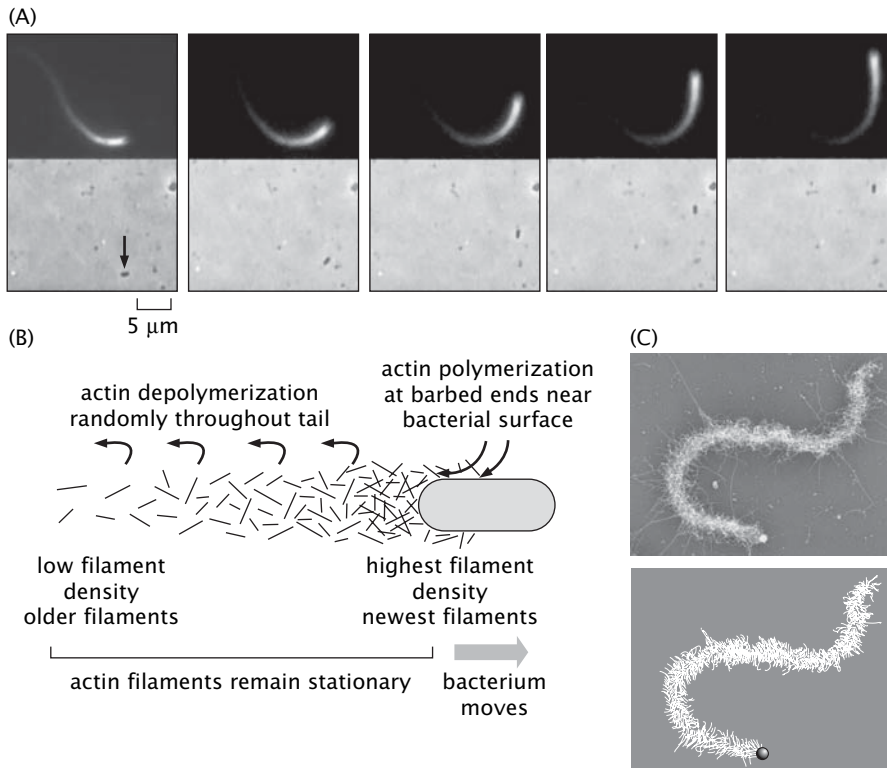


Figure 15.3 Actin polymerization-driven movement of *L. monocytogenes*. (A) This series of time-lapse images shows the movement of a bacterium in a cytoplasmic extract. Phase-contrast images of the bacterium are shown on the bottom in each frame (the bacterium is indicated with an arrow) and fluorescently labeled actin is shown on the top frame. The frames were collected at 30 s intervals. (B) Schematic diagram showing the dynamics of actin filaments in the comet tail. (C) Electron micrograph of plastic bead driven by actin polymerization with schematic shown below. (A, courtesy of D. Fung and J. Theriot; C, courtesy of L. Cameron, T. Svitkina, J. Theriot, and G. Borisy.)

(obviously, this is a gross oversimplification, but nevertheless provides a useful bound), then we estimate that the mean incorporation rate is

$$\frac{dN_{actin}}{dt} \approx \frac{v_{cell}}{L_{monomer}} \approx \frac{200 \text{ nm/s}}{3 \text{ nm}} \approx 60 \text{ monomers/s.} \quad (15.1)$$

Note that this rate of polymerization is very characteristic of cellular polymerization and will serve as a useful rule of thumb in subsequent discussions.

Three notes of caution are in order. First, the actual rate of polymerization is strongly dependent upon the concentration of available subunits as we will explore in more detail later in the chapter. Second, actin polymerization is not the rate determining step for movement of either the keratocyte or *Listeria*. Other forces such as adhesion actually limit their speeds. Third, living cells employ a legion of cytoskeleton-associated proteins to regulate the location and dynamics of actin and the other cytoskeletal filaments. Frequently, the rates of cellular events are determined by the activation and localization of these accessory proteins, rather than actin itself. Nevertheless, this estimate accurately demonstrates that cytoskeletal dynamics must be considered on time scales in which individual events may take place in only tens of milliseconds.

Besides the assembly of the actin structures at the leading edge during cell motility, another dramatic example of regulated actin dynamics is seen during cell division, when a belt of actin and myosin filaments quickly assembles around the center of a cell and contracts to pinch it in half. In the fission yeast, *Schizosaccharomyces pombe*, about 30 accessory factors have been identified that modulate the assembly of actin filaments in the cleavage ring.

Experiments Behind the Facts As stated above, rates for cytoskeletal reactions depend upon the concentrations of the proteins involved. Many proteins are not uniformly distributed throughout the cell and we need to know the local concentration rather than the global average concentration of the protein of interest. For these purposes, merely knowing the number of molecules per cell is not enough, we must also know their spatial distribution. The combination of fluorescence microscopy with other quantitative techniques permits this kind of measurement.

An example of a census of actin-related proteins is shown in Figure 15.4. It is first necessary to determine the total concentration of each protein and then to characterize the distribution of the protein within individual cells. For a large number of proteins believed to play roles in cell division, *S. pombe* strains were generated in which exactly one protein of interest was fused to a yellow fluorescent protein, YFP. In order to determine the number of molecules of each tagged protein present in the cells, the average protein concentration can be measured using a quantitative technique such as Western blotting. In a Western

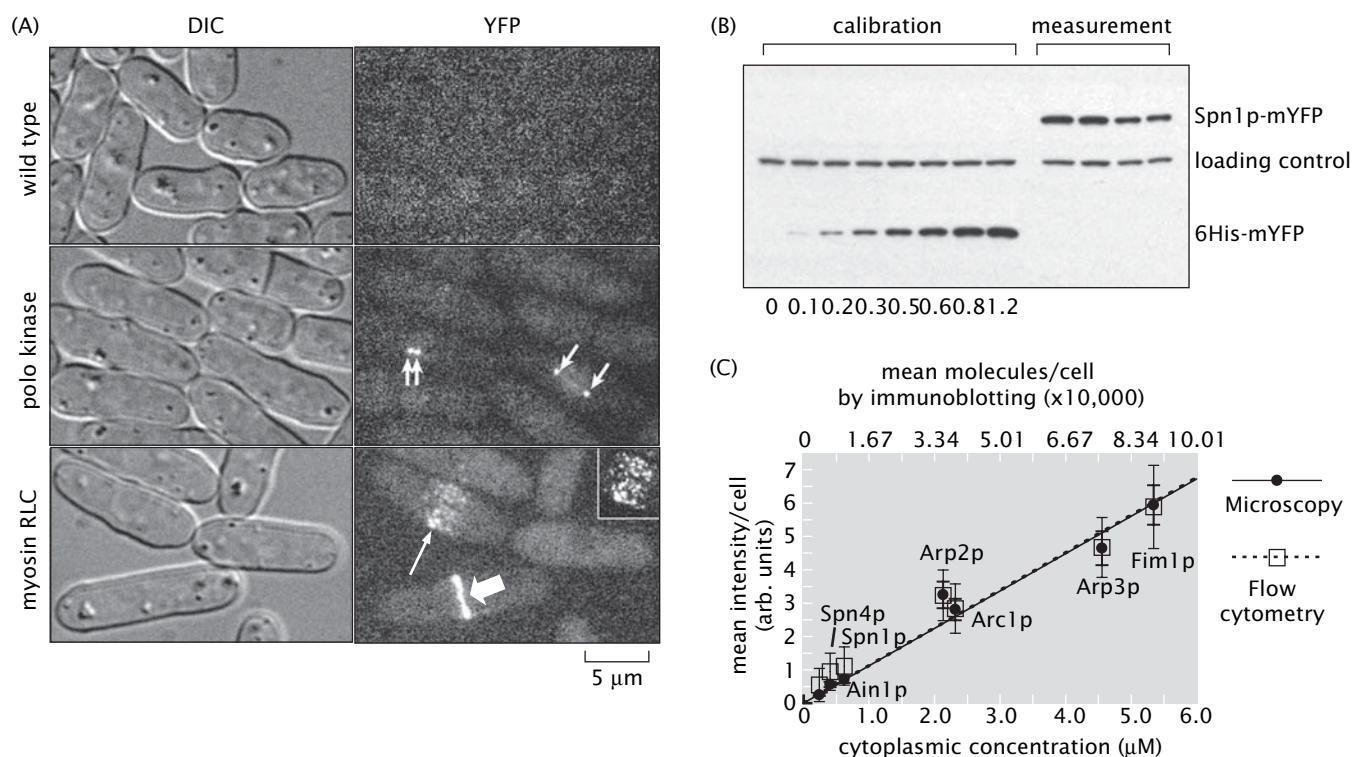


Figure 15.4 Calibration and quantitation of cell-division-associated proteins in the fission yeast *S. pombe*. (A) Wild-type yeast cells, clearly visible as individuals by differential interface contrast microscopy, have no fluorescent signal in the YFP channel. Polo kinase is not visible in most cells, but in two cells caught in the process of chromosome segregation, the kinase is seen concentrated in pairs of dots (small arrows). The myosin regulatory light chain accumulates in a narrow ring as seen in the cell at the bottom of the image (fat arrow), immediately before the cell divides. At a slightly earlier stage in the cell cycle, myosin regulatory light chain begins to accumulate near the presumptive division site in a loose band of dots (long arrow). (B) The average concentration of each protein fusion can be measured using calibrated Western blots. On the left-hand half of the gel, known amounts of purified YFP protein are loaded together with a control protein present in the same amount in every lane. On the right-hand part of the gel, four replicate measurements are made for a single YFP-tagged protein. The amount of the tagged protein is determined by comparing the intensity of the bands to the calibration curve. (C) The number of molecules per cell determined by immunoblotting is linearly related to the average fluorescence intensity per cell measured by flow cytometry or fluorescence microscopy. (A–C, adapted from J.-Q. Wu and T. D. Pollard, *Science*, 310:310, 2005.)

blot the proteins from a large population of cells are all run out together on a gel and then probed with an antibody. A specific antibody against YFP recognizes all of the tagged proteins with equal affinity and the Western blot signal can be calibrated against a known dilution of purified YFP. Dividing this by the number of cells loaded on a gel gives a measurement of the average concentration of each tagged protein per cell. Having calibrated the actual number of molecules per cell using the Western blot, the measured fluorescence intensity (observed either by fluorescence microscopy or by flow cytometry) can be related to an absolute scale of cytoplasmic protein concentration. Finally, local concentrations can be determined from the fluorescence microscopy images. Proteins involved in building the cytokinetic furrow (plane of cell division) are concentrated up to 100 fold on the furrow relative to their global abundance.

15.2 A CHEMICAL PICTURE OF BIOLOGICAL DYNAMICS

We have given a few qualitative descriptions of cases where understanding rates of transformation are critical to understanding biological processes. We now turn to building the quantitative toolkit to treat these cases rigorously. A quantitative theory of such reactions must ultimately answer three key questions about all of the molecular participants: how many molecules are there, where are they, and when are they there?

15.2.1 The Rate Equation Paradigm

The starting point for our discussion is the idea of a chemical concentration. Recall that the concentration tells us the number of molecules of a given species per unit volume (see Figure 13.9 on p. 000). The conventional reason for using a concentration rather than explicitly calling out the *number* of molecules is that the concentration is applicable whether we talk about a drop of water or an entire lake. Further, as we will see below, concentrations (and not absolute particle numbers) often dictate the rates of chemical reactions.

Chemical Concentrations Vary in Both Space and Time

For the purposes of the present discussion, we now imagine that the concentration of the i th species varies with both position and time such that we think of the concentration as $c_i(\mathbf{r}, t)$, which tells us the number of molecules of type i per unit volume at position \mathbf{r} at time t . Exploiting a definition of concentration as a “field variable” (a quantity that varies in space) anticipates the fact that the chemical state of a test tube or a cell can develop spatial nonuniformity (that is, dependence on \mathbf{r}) and time variation. The assumption that makes these ideas tolerable is that the spatial variation of the concentration changes over distances which are large compared to the mean spacing of the molecules themselves. That is, every little box within the overall volume behaves like a box of uniform concentration.

We note that in the context of a living cell, there may be reasons to doubt the validity of the concentration idea itself since (i) the number of molecules can be exceedingly small and (ii) such molecules can be

localized to membranes or particular organelles. Thus it is important to bear two things in mind: first, local concentration rather than global concentration is the appropriate parameter for cases where molecules are confined to particular organelles or regions, and second, for those cases where actual molecular numbers are small, it will be important to consider the stochastic behaviors of individual trajectories rather than global averages. With these provisos, we forge ahead.

Rate Equations Describe the Time Evolution of Concentrations

We begin with the simplest case in which we assume that the concentration at one point in space is identical to that at another. As a result, we drop the label \mathbf{r} in our description of the concentration and focus only on $c_i(t)$ which changes over the course of time as a result of the reactions that link the various reactants, $\{c_j\}$. We introduce the notation $\{c_j\}$ as shorthand for the set $(c_1, c_2, c_3, \dots, c_n)$ where each subscript refers to a different species. The fundamental postulate of the rate equation paradigm is that we can write the time evolution of the concentration in the form of a differential equation as

$$\frac{dc_i(t)}{dt} = f(\{c_j\}; \{k_i\}), \quad (15.2)$$

where $f(\{c_j\}; \{k_i\}) = f(c_1, c_2, \dots, c_n; k_1, k_2, \dots, k_m)$. These various concentrations c_1, c_2, \dots, c_n are for all of the species implicated in the reactions of interest and the parameters k_i are “rate constants” that dictate how fast the various reactions go. Equation 15.2 says that the concentration of the i th species changes in time. How much it will change depends upon the concentrations of all of the various other species which couple to c_i . To make these ideas precise, we now consider explicit examples of different types of reaction which take $f(\{c_j\}; \{k_i\})$ from abstract to concrete form.

15.2.2 All Good Things Must End

Macromolecular Decay can be Described by a Simple, First-order Differential Equation

One of the key physical processes that must be considered when trying to endow the function $f(\{c_j\})$ with real content is the idea that macromolecules decay and are degraded. For example, if we consider the mRNA within a cell, these molecules are generally short-lived in comparison with the average division time of the cell. Similarly, proteins in the cell have a characteristic tendency to decay. The actual lifetime of an individual protein may vary from one kind of protein to another and may be regulated within the cell.

For these decay reactions, just as for radioactive decay, the material does not vanish but rather is transformed into something else. Degraded mRNA is broken down into individual nucleotides and degraded proteins are broken down into individual amino acids. For the purposes of our discussion on rates of decay reactions, we will begin by ignoring these complexities and instead consider the concentration of only one species at a time.

Our principal biological example in this section will be the chemical reaction that lies at the heart of photosynthesis and also vision. A small organic molecule called retinal, illustrated in Figure 15.5, can exist in two slightly different conformational forms. As found in its natural environment associated with a protein in the membrane of photosynthetic

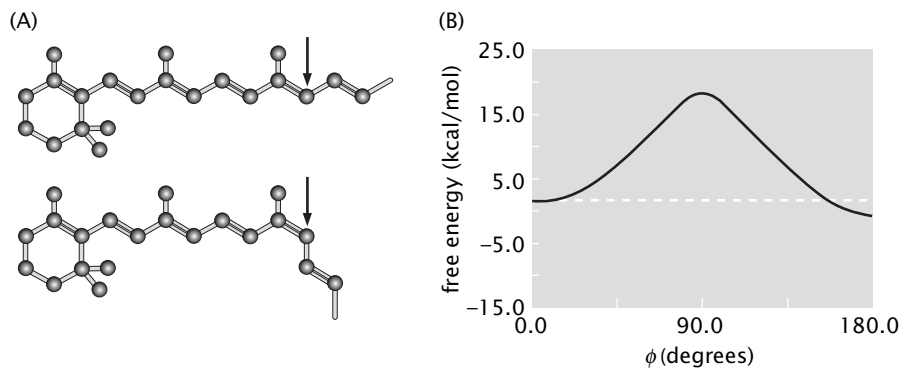


Figure 15.5 The conformational change of retinal. (A) The all-*trans* form of retinal, shown at the top, is its lowest energy state. The 13-*cis* form, shown at the bottom, is formed by rotation around the atom indicated with the arrow. This rotation is commonly caused by absorption of a photon. (B) The calculated energy landscape for retinal as a function of the degree of rotation around the carbon atom reveals a large energy barrier between the *cis* and *trans* forms. (B, adapted from A. Hermone and K. Kuczera, *Biochem.*, 37:2843, 1998.)

bacteria, the lower energy form of retinal, or ground state, is referred to as “all-*trans*-retinal” because of the arrangement of the double bonds in its long tail. A second form, 13-*cis*-retinal, exists in a slightly higher energy state. To go from the all-*trans* form to the 13-*cis* form, one of the carbon–carbon double bonds must undergo a 180° rotation introducing a kink in the middle of the molecule’s tail. In nature, retinal and related molecules can undergo this conformational change (also called an isomerization reaction) when they collide with a photon carrying the appropriate energy. Absorption of the energy from the photon enables retinal to overcome the significant energy barrier for rotation of this double bond as illustrated in Figure 15.5(B). Given sufficient time, the slightly higher energy 13-*cis*-retinal will decay back to the lower energy form of all-*trans*-retinal.

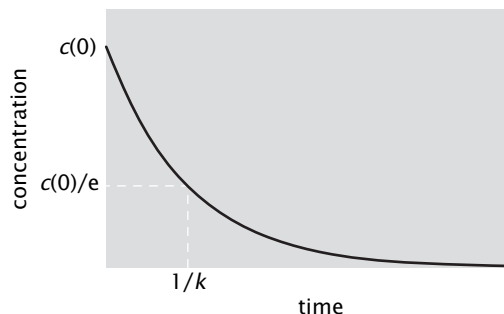
This tiny conformational change is exploited by cells in several remarkable ways. In photosynthetic bacteria, retinal is embedded at the heart of a large transmembrane protein called bacteriorhodopsin. The photon-induced kinking of the retinal is amplified by the protein to generate a large scale conformational change that eventually results in the transport of a single hydrogen ion from the inside of the cell to the outside of the cell. Thus the energy of the photon has been converted into an electrochemical transmembrane gradient which can be used by the bacterium to generate ATP, to spin its flagella, and for any other purpose it desires. In the human retina, protein homologs of bacteriorhodopsin are found in light-sensitive rod and cone cells. Here a slightly different isomerization of retinal (from the 11-*cis* form to the all-*trans* form) initiates a signal transduction cascade which triggers neurons to communicate the change in state to the visual cortex of the brain where we perceive retinal isomerization as light.

Decay reactions like the conversion of 13-*cis* retinal into all-*trans* retinal can be captured very simply using equations of the form of eqn 15.2. In particular, for the case in which we are interested in the simple decay of a given reactant, we have $f(c; k) = -kc$, which says that the rate of decay of the reactant is proportional to how much reactant there is around. The parameter which characterizes that decay rate for a given molecular species is k and the evolution equation itself is

$$\frac{dc(t)}{dt} = -kc(t). \quad (15.3)$$

Note that the constant k which parameterizes the rate of decay has units of 1/time.

Figure 15.6 The number of molecules as a function of time during a decay process. The time scale $1/k$ sets the time it takes before the concentration has decayed to $1/e$ of its initial value.



This linear differential equation can be solved by recourse to the method of separation of variables (see eqn 13.58 on p. 000) and results in a solution of the form $c(t) = c(0)e^{-kt}$, yielding a time-dependent concentration profile of the form

$$c(t) = c_0 e^{-t/\tau}, \quad (15.4)$$

where c_0 is the initial concentration (that is, $c(0) = c_0$) and we have defined a characteristic time $\tau = 1/k$. The time evolution in the concentration of molecules which suffer such decay is shown in Figure 15.6. This simple calculation shows that if we start out with some initial concentration c_0 , this concentration will steadily decline over time with an average exponential profile like that shown in the figure and symbolized in eqn 15.4. A cautionary note is in order: the use of rate equations like those advocated here focuses on the average values of quantities of interest. This automatically deprives us of deeper contact with fluctuational quantities. This is one reason we now turn to considering these processes from the single-molecule perspective.

15.2.3 A Single-Molecule View of Degradation: Statistical Mechanics Over Trajectories

Molecules Fall Apart with a Characteristic Lifetime

As noted above, the simplest mathematical description of decay dynamics is founded upon introducing a characteristic decay constant. It is of interest to examine this decay constant more deeply from both a phenomenological and a microscopic perspective. We adopt the view that the molecule can undergo any of an infinite number of different microscopic trajectories. The idea is that when the system has not yet decayed it is in a state labeled with a 1 and when it has decayed it is labeled with a 0. Here we are generalizing the equilibrium ideas of Chapter 7 to the dynamical case where we consider the transitions between the two states over time. An example of this class of trajectories is shown in Figure 15.7.

Mathematically, we label these trajectories $\sigma_i(t)$, where the trajectory is defined as

$$\sigma_i(t) = \begin{cases} 1 & \text{if } t < t_i \\ 0 & \text{otherwise} \end{cases}, \quad (15.5)$$

where the time t_i is the waiting time associated with the trajectory of interest. The role of the constant k (or alternatively, of $\tau = 1/k$) is to characterize the *average* lifetime of the macromolecule of interest. Because the rate constant k has units of inverse time (for example, s^{-1}) as it describes the probability that something will happen per unit time, its reciprocal τ simply has units of time and can be thought of intuitively

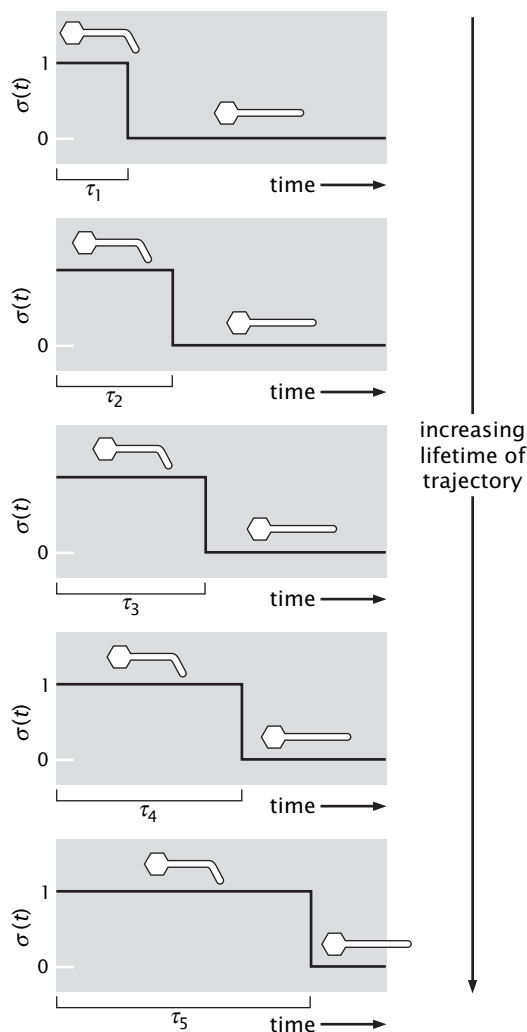


Figure 15.7 Schematic showing the class of microscopic trajectories for a system undergoing simple isomerization/decay dynamics. The two states of the system are labeled by 1 and 0 and hence a given trajectory is characterized by some waiting time in the 1 state followed by a fast decay to the 0 state. The transition itself is assumed to be very fast relative to the waiting time. The set of trajectories shown here provides a few representative examples. The waiting time τ_i is actually a continuous variable so there is a continuum of allowed trajectories.

as dictating the average lifetime of the molecule. That is, a given macromolecule, such as a mRNA, can decay after a waiting time of one second or one minute or one week. However, when we consider a huge collection of such molecules, it makes sense to speak of an average lifetime associated with these molecules and that is what the decay constant captures.

We can use this trajectory picture with our “trajectories and weights” approach introduced in Figure 13.14 (p. 000). We discretize time into N intervals of length Δt (so the total time $t = N\Delta t$) and then find the probability of a given trajectory by multiplying the probabilities of what happens at each time step over the entire trajectory. For example, if the molecule survives for N time steps and decays on the $(N + 1)$ th time step, then the probability of that process is

$$p(t)\Delta t = \underbrace{(1 - k\Delta t) \times (1 - k\Delta t) \times \cdots (1 - k\Delta t)}_{N \text{ time steps}} \times k\Delta t, \quad (15.6)$$

where $k\Delta t$ is the probability of a decay during any time step and $(1 - k\Delta t)$ is the probability of no decay at a given time step. The function $p(t)$ is a probability density and requires that we compute $p(t)\Delta t$ to compute the probability that the decay occurs between time t and $t + \Delta t$. If we

use the fact that $\Delta t = t/N$, this result can be rewritten as

$$p(t)\Delta t = (1 - k\Delta t)^N k\Delta t = \left(1 - \frac{kt}{N}\right)^N k\Delta t \approx ke^{-kt}\Delta t, \quad (15.7)$$

where we have used the identity that $e^{-x} = \lim_{N \rightarrow \infty} (1 - x/N)^N$. This result tells us that once we have set the mean lifetime ($\tau = 1/k$), the probability of decay in the time interval between t and $t + \Delta t$ is

$$p(t)\Delta t = \frac{1}{\tau} e^{-t/\tau} \Delta t. \quad (15.8)$$

Decay Processes can be Described with Two-state Trajectories

Another way of illustrating the trajectory perspective for decay processes is to exploit the maximum entropy approach introduced in Section 6.1.5 (p. 000). Recall that each decay process is characterized by a trajectory corresponding to how long the system is in state A before decaying to state B. It is convenient to characterize the molecular state with the discrete index 1 for state A and 0 for state B. Our aim here is to use the information theoretic approach to statistical mechanics introduced in Section 6.1.5 (p. 000) to obtain the probability distribution on these trajectories. Just as our discussion in Chapter 6 showed several ways to obtain the Boltzmann distribution, our present discussion illustrates several distinct ways of deriving the waiting time distribution, $p(t)$.

We are interested in the probability $p(t)$ which signifies the probability of a microtrajectory with lifetime t , precisely the same quantity considered in eqn 15.8. The only information about the overall process that we invoke in our analysis is that the average lifetime is τ . In light of this constraint, we can write the constrained Shannon entropy functional as

$$S = - \underbrace{\int_0^\infty p(t) \ln p(t) dt}_{\text{Shannon entropy}} - \lambda \underbrace{\left(\int_0^\infty p(t) dt - 1 \right)}_{\text{normalization constraint}} - \mu \underbrace{\left(\int_0^\infty tp(t) dt - \langle t \rangle \right)}_{\text{average lifetime constraint}}. \quad (15.9)$$

More concretely, the constraints captured with the Lagrange multipliers above are

$$\int_0^\infty p(t) dt = 1, \quad (15.10)$$

which specifies that the probabilities sum to 1, and

$$\int_0^\infty tp(t) dt = \tau, \quad (15.11)$$

which guarantees that the average lifetime is τ . Refer to “The Math behind the Models” on p. 000 for a reminder on the Lagrange multiplier concept. As usual, we are now faced with the prospect of maximizing this constrained Shannon entropy by equating its derivative to zero and solving for $p(t)$, resulting in

$$-\ln p(t) - \lambda - 1 - \mu t = 0. \quad (15.12)$$

This results in an expression for the probability of a trajectory with lifetime t of

$$p(t) = e^{-1-\lambda} e^{-\mu t}. \quad (15.13)$$

Now, we have to impose the constraints in order to determine the Lagrange multipliers λ and μ . The normalization constraint results in the condition

$$\int_0^{\infty} p(t) dt = e^{-1-\lambda} \underbrace{\int_0^{\infty} e^{-\mu t} dt}_{=1/\mu} = 1. \quad (15.14)$$

As a result of this analysis, we have

$$e^{-1-\lambda} = \mu. \quad (15.15)$$

Given that we have the normalization of the probability distribution in hand which leads us to

$$p(t) = \mu e^{-\mu t}, \quad (15.16)$$

we now determine the second Lagrange multiplier by exploiting the average lifetime, $\tau = \int_0^{\infty} t p(t) dt$. In light of our determination of the first Lagrange multiplier, this condition results in

$$\tau = \mu \int_0^{\infty} t e^{-\mu t} dt. \quad (15.17)$$

We can now perform this integration by recourse to the simple trick of differentiating with respect to μ to bring the factor t into the integrand (introduced in the “Tricks behind the Math” on p. 000), resulting in

$$\tau = \mu \left(-\frac{d}{d\mu} \right) \int_0^{\infty} e^{-\mu t} dt = \mu \left(-\frac{d}{d\mu} \right) \frac{1}{\mu} = \frac{1}{\mu}. \quad (15.18)$$

Hence our second Lagrange multiplier μ is now determined as $\mu = 1/\tau$. Substituting this result into eqn 15.16 yields $p(t) = (1/\tau) e^{-t/\tau}$, leading in turn to the result that the probability that the decay will occur between times t and $t + \Delta t$ is given by

$$p(t)\Delta t = \frac{1}{\tau} e^{-t/\tau} \Delta t. \quad (15.19)$$

We will come back to this in the context of molecular motors when analyzing the different lifetimes of a motor’s internal states (see Section 16.2.3 on p. 000).

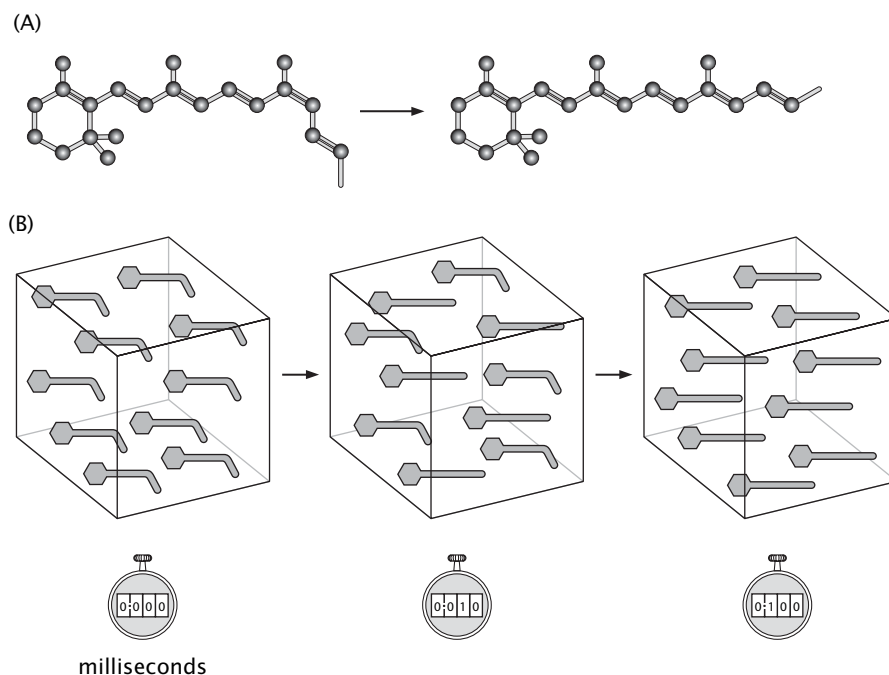
Decay of One Species Corresponds to Growth in the Number of a Second Species

The reactions we have been thinking about are described by the simple chemical formula



This kind of process is depicted schematically in Figure 15.8 for the example of retinal. Thus far, we have considered only the fate of species A, but of course in the real reaction the number of molecules of the product species B also changes with time and the time-dependent equations

Figure 15.8 Different views of the isomerization process. (A) Schematic of an isomerization process where species A is decaying into species B. In this case we use the two forms of retinal described earlier in the chapter to characterize the process. (B) Schematic of the change in the populations of the two species over time.



describing the fates of A and B are inextricably linked to one another. In this case, for every decrease in the number of A molecules we have a corresponding increase in the number of B molecules which implies the constraint

$$c_A(t) + c_B(t) = c_0. \quad (15.21)$$

Indeed, the dynamics of these two species as embodied in eqn 15.21 is nothing more than an expression of mass conservation. The condition of mass conservation implies that

$$\frac{dc_A}{dt} = -\frac{dc_B}{dt} = -kc_A. \quad (15.22)$$

If we consider the situation where initially all of the molecules are A molecules, then we have $c_A(0) = c_0$ and $c_B(0) = 0$. From our earlier solution of the decay problem, it is now straightforward to write down the time evolution of both species. Using the mass conservation condition given in eqn 15.21 we find

$$\frac{dc_B}{dt} = kc_A = k(c(0) - c_B) \Rightarrow c_B(t) = c_0(1 - e^{-kt}). \quad (15.23)$$

The time evolution of both populations under these initial conditions is indicated schematically in Figure 15.8 and the reader is asked to flesh out this solution and make the corresponding plots in the problems at the end of the chapter.

The same ideas introduced above can be used just as well for examining the reversible reaction



In this case, the rate equations of interest can be written as

$$\frac{dc_A}{dt} = -k_+c_A + k_-c_B \quad (15.25)$$

and

$$\frac{dc_B}{dt} = -\frac{dc_A}{dt}, \quad (15.26)$$

with the constraint of mass conservation of the form given in eqn 15.21. Equation 15.25 says that the change in concentration of species A comes from two sources: (i) the decay of A into B with rate constant k_+ and (ii) the decay of B into A with rate constant k_- . In this case, the long-time behavior is nonzero concentrations of both A and B, with their ratio dictated by the ratio k_+/k_- . The details of this analysis are left to the reader in the problems.

15.2.4 Bimolecular Reactions

Chemical Reactions Can Increase the Concentration of a Given Species

Decay and isomerization are only a limited subset of the repertoire of interesting biochemical transactions. Indeed, these reactions are unusual in that there is only one molecule involved; this one molecule may change its state, but does not explicitly interact with other molecules. In general, the more interesting cases are those in which two different reactants come together to form some third product. In these cases, the function $f((c_j))$ must have contributions coming from the presence of interactions between the different reactants. In particular, we now consider reactions of the form



As before, our interest is in finding a description which provides us with the concentrations of both reactants and products as a function of time.

Intuitively, we can argue that the contribution of the association reaction to the overall concentration of the products can be written as

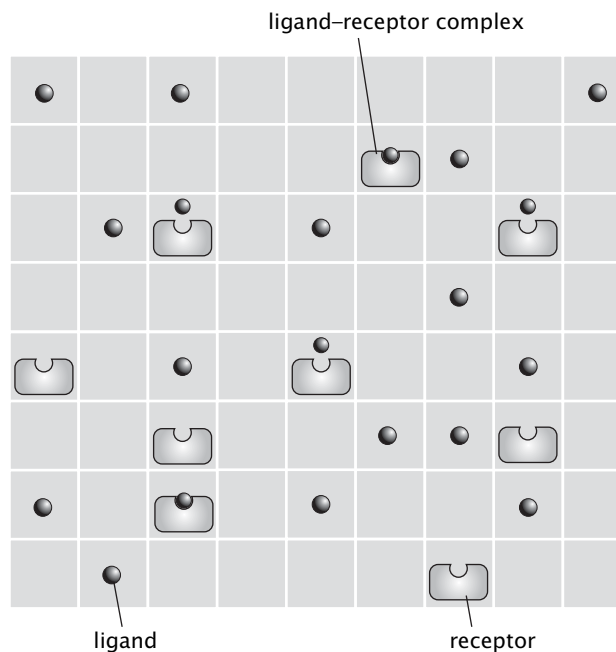
$$\frac{dc_{AB}(t)}{dt} = k_{AB}c_Ac_B, \quad (15.28)$$

where k_{AB} is a constant that reflects the rate of association of A and B molecules. Conceptually, this equation says that A and B molecules come together to form AB molecules and the rate at which they do so is proportional to the probability that As and Bs are at the same place (that is, their concentrations). Note that bimolecular reactions lead to a new feature in our description. In particular, we note that the dynamical equations of different species are coupled. In our earlier treatment of decay reactions, the equation for $c_A(t)$ made no appeal to the concentrations of other species. In the present case, changes in the concentration of one species are accompanied by a concomitant change in the concentrations of other species. Mathematically, this amounts to the fact that the differential equations for the system are *coupled* (in more than the simple way revealed in eqn 15.22).

To see how this works more concretely, we return to one of our workhorse problems, namely, ligand–receptor binding, and now explicitly consider how the system changes over time. We consider a ligand and receptor whose concentrations are [L] and [R], which are either free in solution or bound in the LR complex whose concentration is [LR]. To model the reaction



Figure 15.9 Lattice model of ligand–receptor binding dynamics. The system is divided up into Ω distinct boxes. There are L ligands and R receptors in solution and the binding reaction between them to form the complex LR can occur when a ligand and receptor are found at the same lattice site. When a ligand and receptor are found in the same box, the probability that they will react to form LR in time Δt is given by $k'_{on}\Delta t$.



we consider a lattice model as shown in Figure 15.9 in which there are a total of Ω distinct “lattice” sites, L ligands and R receptors. We treat the solution as an ideal solution of ligand and receptor where the probability of occupancy of an elementary box by ligand is L/Ω , and the probability of occupancy of a box by receptor is R/Ω . Furthermore we assume that for L and R to form a complex they must be in the same box. Given these assumptions, in time Δt , the change in the number of ligand–receptor complexes due to binding of ligand to receptor can be written as

$$\Delta N_{LR} = \underbrace{-(k_{off}\Delta t)N_{LR}}_{\text{decay term}} + \underbrace{\Omega}_{\text{no. of boxes}} \times \underbrace{\frac{N_L}{\Omega} \frac{N_R}{\Omega}}_{\text{box occupancy prob.}} \times (k'_{on}\Delta t), \quad (15.30)$$

where the first term is the decay process discussed earlier (see Section 15.2.2 on p. 000), while the second term represents the rate at which LR is produced and is obtained by working out the rate per elementary box times the total number of such boxes; k'_{on} is the rate at which ligand–receptor pairs that are colocalized in the same elementary box transform to a ligand–receptor complex.

This result can be recast in the more familiar differential form by dividing the left- and right-hand sides by Δt and then by the volume Ωv , where v is the volume of the elementary box in our lattice model. In particular, we have

$$\frac{d}{dt} \left(\frac{N_{LR}}{\Omega v} \right) = -k_{off} \left(\frac{N_{LR}}{\Omega v} \right) + \frac{\Omega}{\Omega v} \frac{N_L}{\Omega v} \frac{N_R}{\Omega v} v^2 k'_{on}, \quad (15.31)$$

where in the second term on the right we have divided and multiplied by v twice in order to convert to concentration variables such as $[L] = N_L/\Omega v$, $[R] = N_R/\Omega v$ and $[LR] = N_{LR}/\Omega v$. These manipulations transform eqn 15.30 into

$$\frac{d[LR]}{dt} = -k_{off}[LR] + k_{on}[L][R], \quad (15.32)$$

where the bimolecular on-rate is related to the lattice model rate constant by $k_{on} = \nu k'_{on}$, and has units of $M^{-1} s^{-1}$. This heuristic derivation shows how to link simple lattice models with macroscopic rate equations defined in terms of concentration variables.

Equilibrium Constants Have a Dynamical Interpretation in Terms of Reaction Rates

The rate-equation formalism described above provides a useful opportunity to make contact with what we already know about the equilibria of reactions. In particular, by definition, equilibrium is a reflection of the fact that the reaction has reached a steady state where the concentrations are no longer changing over time because the forward flux in the reaction exactly balances the backwards flux. It is important to note that individual molecules are still undergoing the reactions, but the net number of transformations in each direction is equal so the overall concentration does not change. We can express this idea mathematically as $d[LR]/dt = 0$, resulting in

$$-k_{off}[LR]_{eq} + k_{on}[L]_{eq}[R]_{eq} = 0. \quad (15.33)$$

This equation provides a relation between the equilibrium concentrations ($[L]_{eq}$, $[R]_{eq}$, $[LR]_{eq}$) and the relevant rate constants, namely,

$$K_d = \frac{[L]_{eq}[R]_{eq}}{[LR]_{eq}} = \frac{k_{off}}{k_{on}}. \quad (15.34)$$

Using our rate-equation picture, we have recovered the law of mass action derived using statistical mechanics in Section 6.3 (p. 000) where we demonstrated that K_d is the concentration at which $p_{bound} = 1/2$. This equation demonstrates the connection between the equilibrium concentrations and the associated kinetic rate constants. However, as indicated schematically in Figure 15.10, the rate picture allows us to say much more than what the terminal, privileged (equilibrium) state will be. The dynamical picture captured by the rate equations permits us to examine the variation in the concentrations over time for different choices of their initial values (that is, at time $t = 0$).

15.2.5 Dynamics of Ion Channels as a Case Study

An interesting application of the ideas developed so far is the dynamics of ion channels. In Chapter 7, we discussed ion channels as an example of a real biological system that can be fruitfully viewed using the two-state paradigm because in the simplest picture, they exist only in open or closed states (see Figure 7.2, p. 000). There we considered channel behavior only from an equilibrium perspective and now we are ready to turn to the question of rates. For example, when the membrane of a nerve cell is depolarized, how long does it take for the voltage gated calcium channels to open, and how does the time-dependent behavior of the ion distribution along the whole membrane depend on the behavior of the individual channels themselves? Our goal is to write a rigorous description that relates the trajectories of individual channels, which are intrinsically binary, to the overall behavior of a large scale system which may have an analog-like response. In addition, we explore a probabilistic description of how the behavior of identical channel molecules may differ over time. We will model the channel as existing in only two states, open and closed, with only a single relevant transformation

Figure 15.10 Direction of reaction. (A) Time evolution of the system in the case in which the initial concentrations of [L] and [R] are in excess of their equilibrium concentrations. (B) Time evolution of the system in which the initial concentration of [LR] is in excess of its equilibrium concentration.

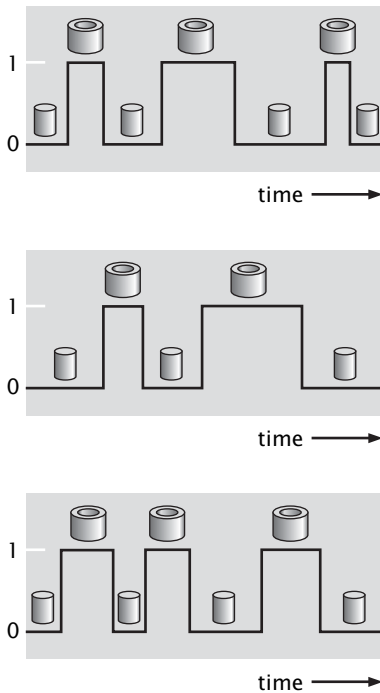
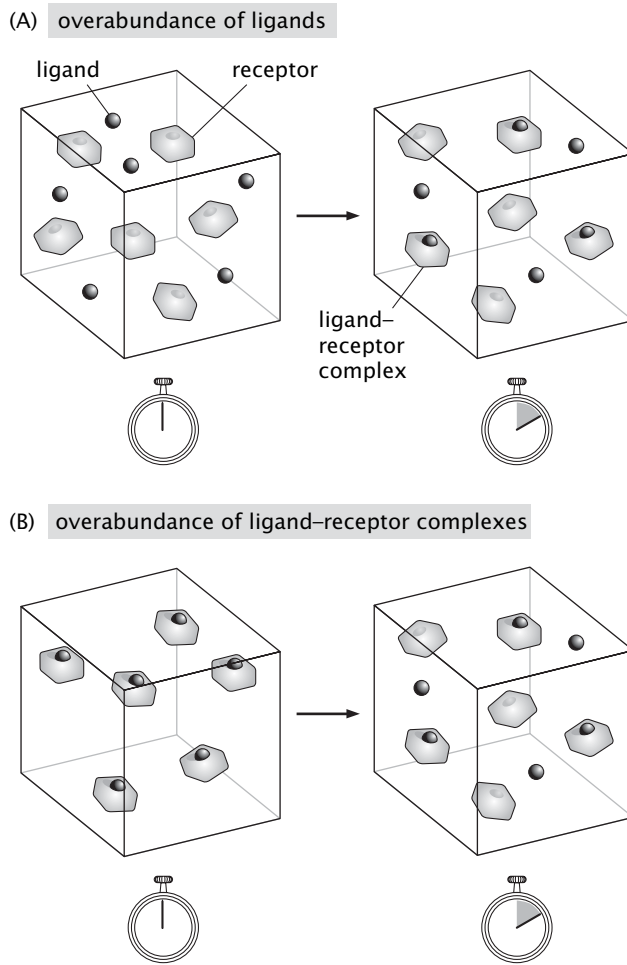


Figure 15.11 Ion channel trajectories. Three representative examples of the time evolution of a two-state ion channel which switches back and forth between the closed and open states. For simplicity, we assume that the switching itself is *instantaneous* in comparison with the time spent in either of the two states. The icons represent the open and closed states.

reaction converting one state into the other. This will be a warm-up problem for more complex systems later in the chapter that involve more molecular species and more complex transformations.

Rate Equations for Ion Channels Characterize the Time Evolution of the Open and Closed Probability

Examples of the microtrajectories available to individual channels are shown in schematic form in Figure 15.11. Our goal is to write a kinetic description which allows us to classify and analyze different trajectories. One quantity we might like to use to characterize ion channel dynamics is the probability that, if we start in the open state at time $t = 0$, it will still be open a time τ later.

To exploit our rate-equation paradigm for the problem of ion channel dynamics, we appeal to Figure 15.12. The idea is that we have a patch of membrane that is occupied by a total of N distinct two-state channels. Our goal is to write a rate equation that characterizes the time evolution of the probability of being in the open state and the way we will do this is to compute $N_O(t)/N$ (where $N_O(t)$ is the number of open channels at time t) which will effectively determine that probability. We adopt a strategy in which time is discretized into steps of length Δt and at each time step, the channel can undergo a transition from its current state or it can remain in the same state. The “reaction” of interest is of the

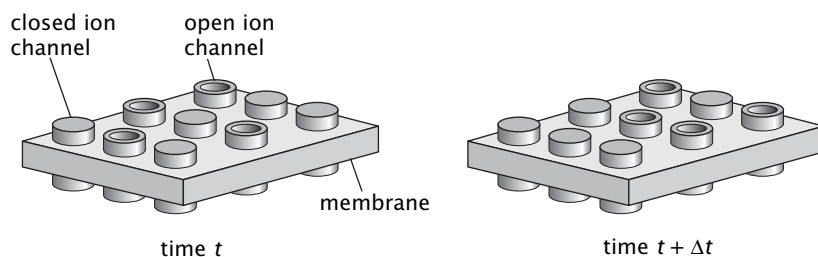


Figure 15.12 Channel gating kinetics. A patch of membrane with a collection of ion channels, some of which are open, some of which are closed. At every time step, channels can either switch their state or stay in the same state.

form



where O signifies the open state, C signifies the closed state and k_+ and k_- are the rate constants that determine the probability of a change of state during a given time step. The change in the number of open channels in a given time step can be written as

$$\Delta N_O = \underbrace{-k_+ N_O \Delta t}_{O \rightarrow C} + \underbrace{k_- N_C \Delta t}_{C \rightarrow O}. \quad (15.36)$$

If we divide both sides by Δt we find the rate of change in the number of open channels as

$$\frac{\Delta N_O}{\Delta t} = -k_+ N_O + k_- N_C, \quad (15.37)$$

which can be further simplified by dividing this equation by N itself and using $p_O = N_O/N$ and $p_C = N_C/N$. If we examine the limit as $\Delta t \rightarrow 0$, this results in the differential equation

$$\frac{dp_O}{dt} = -k_+ p_O + k_- p_C. \quad (15.38)$$

If we now exploit the fact that $p_O + p_C = 1$, which amounts to the statement that the channels are either open or closed (that is, it is a two-state system) this may be rewritten as

$$\frac{dp_O}{dt} = -k_+ p_O + k_- (1 - p_O). \quad (15.39)$$

This equation is more transparent if written in the form

$$\frac{dp_O}{dt} = -(k_+ + k_-) p_O + k_-. \quad (15.40)$$

In particular, we can solve this equation by resorting to separation of variables and by adding a constant term, resulting in

$$p_O(t) = \frac{k_-}{k_+ + k_-} + A e^{-(k_+ + k_-)t}. \quad (15.41)$$

The specific solution cancels off the constant term in the differential equation and the exponential term captures the time dependence. If we now exploit the initial condition that $p_O(0) = 1$ (that is, all the channels are open at $t = 0$), we can determine the constant A resulting in

$$p_O(t) = \frac{k_-}{k_+ + k_-} + \frac{k_+}{k_+ + k_-} e^{-(k_+ + k_-)t}. \quad (15.42)$$

The dynamics of the channel is usefully characterized using this probability which we will show below can also be thought of as providing the *correlation function*. In particular, this solution tells us how to view trajectories like that given in Figure 15.11 with particular reference to how long the channel stays in the closed and open states between switching events. Consider a single-molecule experiment in which we observe a channel switching back and forth between the closed and open states (experimental data of this kind are shown in Figure 7.2 on p. 000). Imagine we start our stopwatch when the protein is in the open state, and we record the state of the protein in time, assigning 0 to the closed state and 1 to the open state. This will result in a random telegraph signal $\sigma(t)$ like that shown schematically in Figure 15.11. Our task is to compute the correlation function $\langle \sigma(0)\sigma(t) \rangle$. The average can be computed by repeating the experiment over and over again; the figure shows the hypothetical outcomes of three such experiments. Alternatively, we could watch a single channel over a long time period and compute a time average. In the case of a stationary process the two procedures give the same result. For a stationary process the random graph you get by shifting $\sigma(t)$ is just as good as the original, that is, it is drawn from the same distribution.

For a *given* process $\sigma(t)$ the quantity $\sigma(0)\sigma(t)$ is either 1 or 0. The average $\langle \sigma(0)\sigma(t) \rangle$ is therefore equal to the probability of $\sigma(t)$ being 1, *conditioned on* $\sigma(0)$ being equal to 1. But this is precisely the probability $p_O(t)$ that we computed above. Experimentally, one way to evaluate these probabilities is to examine channel trajectories like those shown in Figure 7.2 (p. 000) and to make a histogram of the number of times each waiting time (in the interval t and $t + \Delta t$, where Δt is the bin size) appears. Experimental data of this variety for a sodium channel are shown in Figure 15.13.

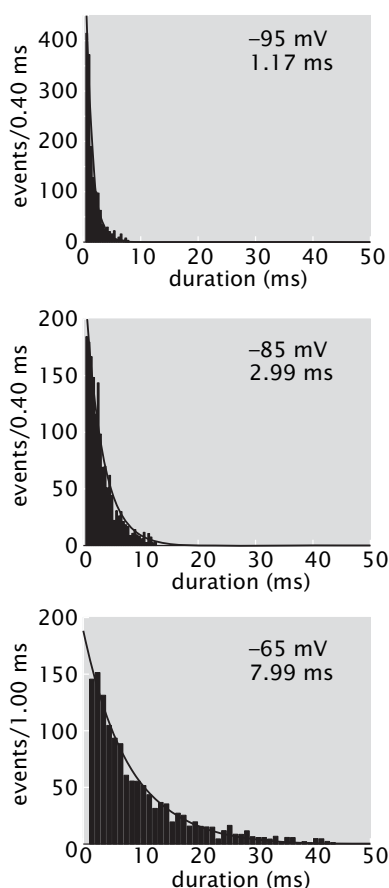


Figure 15.13 Measured channel gating kinetics. Each histogram shows the number of events observed for the open state lifetime for a voltage-gated sodium channel. The frequencies shown on the y-axis are given as number of events per bin size (measured in milliseconds). Note that the bin size is larger for the bottom graph. The three histograms correspond to different membrane voltages as indicated in the figure. The average lifetime τ is shown for each voltage. (Adapted from B. U. Keller et al., *J. Gen. Physiol.*, 88:1, 1986.)

15.2.6 Rapid Equilibrium

Having flexed our muscles with relatively simple two-state ion channels, we are now ready to turn to more complex biological systems that involve multiple transformations. One useful exercise we are now prepared for is to return to the discussion of Section 5.2.1 (p. 000). The goal of that discussion was to assess the circumstances under which we can get away with approximating a nonequilibrium process using equilibrium ideas. Despite the fact that the physics of life is typically portrayed as strictly the province of nonequilibrium thinking, there are many instances in which equilibrium ideas are quite useful. Further, we argued that the question of whether or not equilibrium ideas are appropriate is ultimately a question of time scales. The goal of the present discussion is to use rate equations that explicitly account for the changes in concentration with time so that we can determine whether equilibrium assumptions are appropriate for a particular experiment.

Here we illustrate this idea using a toy model of three chemical species interconverting between one another, with two fast and one slow step characterized by the reaction scheme



We wish to compute the concentration of the three species as a function of time, starting from a state where we have species A only. The fast steps have rate constants $k_{\pm} \gg r$. Also, we simplify the kinetic scheme

by assuming that the $B \rightarrow C$ reaction is irreversible. (A more careful treatment would keep the $C \rightarrow B$ rate and then analyze the solutions by assuming it to be much smaller than all the other ones in the problem.) Our goal is to show that in this explicitly dynamical situation, equilibrium is established rapidly, and thereafter maintained between the fast steps of the reaction.

Some Chemical Reactions Are Linked Together in a Sequence Resulting in Coupled Rate Equations

Based on the kinetic scheme outlined in eqn 15.43 the rate equations for the three chemical species are

$$\begin{aligned}\frac{dA}{dt} &= -k_+A + k_-B, \\ \frac{dB}{dt} &= k_+A - (k_- + r)B, \\ \frac{dC}{dt} &= rB.\end{aligned}\tag{15.44}$$

These can be written in dimensionless form by dividing both sides of the equation by k_- , which effectively corresponds to measuring time in units of $1/k_-$. We introduce the dimensionless time $\tau = k_-t$. It is unfortunate that the conventional notation for dimensionless time τ uses the same symbol as the conventional notation for average lifetime introduced earlier in the chapter. Throughout the remainder of this section τ will be used to refer to dimensionless time. By additionally introducing the dimensionless rate constants $k = k_+/k_-$ (this is also the equilibrium constant for the $A \rightleftharpoons B$ reaction), and $\epsilon = r/k_-$, we can rewrite the rate equations as

$$\begin{aligned}\frac{dA}{d\tau} &= -kA + B, \\ \frac{dB}{d\tau} &= kA - (1 + \epsilon)B, \\ \frac{dC}{d\tau} &= \epsilon B.\end{aligned}\tag{15.45}$$

Since the first two equations are decoupled from the third we solve those using the matrix method, with initial condition $(A(0), B(0)) = (1, 0)$. In matrix form, the above rate equations can be written as

$$\frac{d}{d\tau} \begin{pmatrix} A \\ B \end{pmatrix} = \begin{pmatrix} -k & 1 \\ k & -(1 + \epsilon) \end{pmatrix} \begin{pmatrix} A \\ B \end{pmatrix}.\tag{15.46}$$

The general solution to this matrix equation is

$$\begin{pmatrix} A \\ B \end{pmatrix}(\tau) = a_1 \begin{pmatrix} A_1 \\ B_1 \end{pmatrix} e^{\omega_1\tau} + a_2 \begin{pmatrix} A_2 \\ B_2 \end{pmatrix} e^{\omega_2\tau},\tag{15.47}$$

where $\begin{pmatrix} A_{1,2} \\ B_{1,2} \end{pmatrix}$ are the eigenvectors of the 2×2 matrix in eqn 15.46, while $\omega_{1,2}$ are the corresponding eigenvalues; $a_{1,2}$ are the integration constants which we will determine from the initial conditions. The “Math behind the Models” below summarizes how matrices can be manipulated to find the eigenvalues and eigenvectors.

The eigenvalues of our matrix are solutions to the equation

$$\det \begin{pmatrix} -k - \omega & 1 \\ k & -(1 + \epsilon) - \omega \end{pmatrix} = 0,\tag{15.48}$$

which, once the determinant is resolved, becomes a quadratic equation

$$\omega^2 + (1 + k + \epsilon)\omega + k\epsilon = 0, \quad (15.49)$$

in the unknown eigenvalues ω . The two solutions of the quadratic equation,

$$\omega_{1,2} = -\frac{1}{2}(1 + k + \epsilon) \pm \frac{1}{2}\sqrt{(1 + k + \epsilon)^2 - 4k\epsilon} \quad (15.50)$$

are the eigenvalues which dictate the time evolution of the various concentrations.

To simplify the arithmetic let us make good use of the assumptions we made at the beginning: that k is of order 1 and that ϵ is much smaller than 1. In this case we can Taylor expand eqn 15.50 in powers of ϵ using the rule that $\sqrt{1+x} \approx 1+x/2$ (see “The Math behind the Models” on p. 000) to obtain approximate values of the eigenvalues,

$$\omega_1 = -\frac{k}{k+1}\epsilon, \quad \omega_2 = -(k+1) \quad (15.51)$$

to leading order in ϵ . The lowest-order term in the first eigenvalue is of order ϵ^1 , while the lowest-order term in the second eigenvalue is of order ϵ^0 . It is interesting to note that we obtain a slow ($\omega_1 \ll 1$) and a fast ($\omega_2 \sim 1$) rate, as expected. In particular, the fast rate should correspond to the rate at which equilibrium is established between species A and B, while we expect the slow rate to describe the overall decay of A and B giving rise to chemical species C.

In order to complete the calculation, we still need to compute the eigenvectors corresponding to the eigenvalues ω_1 and ω_2 . These are obtained by solving the following 2×2 system of linear equations:

$$\begin{pmatrix} -k - \omega_{1,2} & 1 \\ k & -(1 + \epsilon) - \omega_{1,2} \end{pmatrix} \begin{pmatrix} A_{1,2} \\ B_{1,2} \end{pmatrix} = 0, \quad (15.52)$$

here written in matrix form. To leading order in ϵ the eigenvectors are

$$\begin{pmatrix} A_1 \\ B_1 \end{pmatrix} = \begin{pmatrix} 1 \\ k \end{pmatrix}, \quad \begin{pmatrix} A_2 \\ B_2 \end{pmatrix} = \begin{pmatrix} 1 \\ -1 \end{pmatrix} \quad (15.53)$$

and the general solution of the differential equation, eqn 15.46 is

$$\begin{pmatrix} A \\ B \end{pmatrix}(\tau) = a_1 \begin{pmatrix} 1 \\ k \end{pmatrix} e^{-(k\epsilon/(k+1))\tau} + a_2 \begin{pmatrix} 1 \\ -1 \end{pmatrix} e^{-(k+1)\tau}. \quad (15.54)$$

Finally, to obtain the integration constants $a_{1,2}$ we make use of the initial condition, $\begin{pmatrix} A \\ B \end{pmatrix}(0) = \begin{pmatrix} 1 \\ 0 \end{pmatrix}$, which when substituted into eqn 15.54 gives

$$\begin{aligned} a_1 + a_2 &= 1, \\ ka_1 - a_2 &= 0. \end{aligned} \quad (15.55)$$

The solution to this set of linear equations is $a_1 = 1/(k+1)$ and $a_2 = k/(k+1)$, and we can now write the full solution of the rate equations for species A and B as

$$\begin{pmatrix} A \\ B \end{pmatrix}(\tau) = \begin{pmatrix} 1/(k+1) \\ k/(k+1) \end{pmatrix} e^{-(k\epsilon/(k+1))\tau} + \begin{pmatrix} k/(k+1) \\ -k/(k+1) \end{pmatrix} e^{-(k+1)\tau}. \quad (15.56)$$

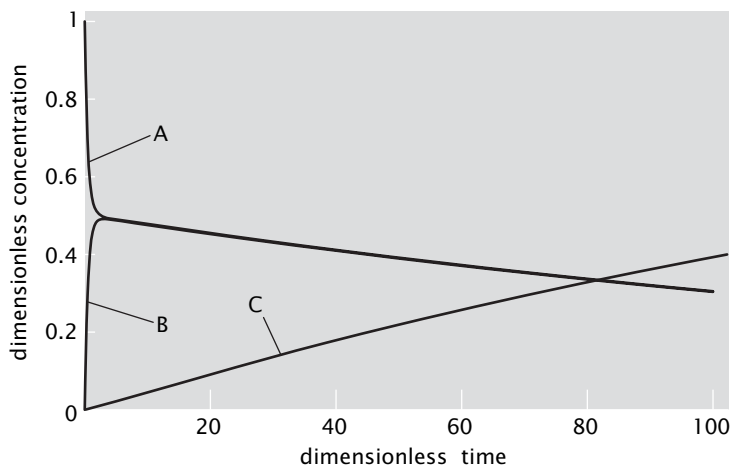


Figure 15.14 The time variation of the concentrations of chemical species A and B, for $k = 1$ and $\epsilon = 0.01$. Initially there is one unit of concentration of A and none of B. After a fast decay of A and rise of B, the two settle into an equilibrium situation where $A = B$. The accumulation of product C is also shown in the figure.

This solution confirms our intuition. In Figure 15.14 we show the exact solution of the rate equations, for parameters $k = 1$ and $\epsilon = 0.01$. As anticipated, we observe a fast decay away from the initial state (all A) until the concentrations of A and B are in a fixed ratio (that is, the equilibrium constant) which is followed by a slow decay during which the species A and B are in equilibrium with each other, but their overall quantity is decaying. In particular, for times such that $\tau \gg 1/(k + 1)$, we can ignore the second term in eqn 15.56 and

$$\begin{pmatrix} A \\ B \end{pmatrix}(\tau) = \begin{pmatrix} 1/(k+1) \\ k/(k+1) \end{pmatrix} e^{-(k\epsilon/(k+1))\tau}. \quad (15.57)$$

This equation describes a slow (rate $\sim \epsilon$) overall decay of species A and B, while their relative concentrations are related by the equilibrium constant: $B(t)/A(t) = k$. What this exercise illustrates is the way in which a dynamical process involving multiple reactions can have some subset of reactions which behave as though they are in instantaneous equilibrium at all times. The classic example of this kind of thinking is its application to reactions catalyzed by enzymes, generally referred to Michaelis–Menten kinetics.

The Math behind the Models: Eigenvalues and Eigenvectors

We are all familiar with equations of the form $ax + b = 0$, where a and b are parameters and x is an unknown. The temptation is to say that the solution of this equation is $x = -b/a$. This is certainly true if a is not zero. If, on the other hand, $a = 0$, then either there is no solution for $b \neq 0$ or any number x is a solution for $b = 0$. These might seem like mathematical niceties, but when a is promoted to a matrix and $b = 0$ the question of when the above equation has nonzero solutions is at the heart of a number of interesting problems, and in particular the one we are about to face, finding the eigenvectors and eigenvalues of a matrix.

We concern ourselves with square matrices, so that the number of rows and the number of columns are the same. We further specialize to 2×2 matrices so as to simplify the algebra, but all our conclusions will apply to matrices of arbitrary size.

The action of a matrix on a vector is illustrated in Figure 15.15. Multiplying a matrix and a vector produces a new vector, which is in general related to the original one by rotating



MATH

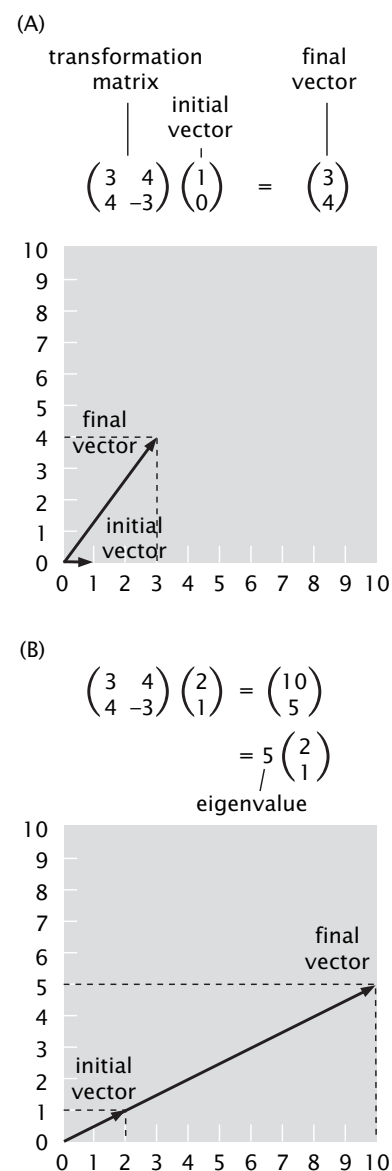


Figure 15.15 Eigenvectors and eigenvalues of a matrix. (A) A matrix acting on an arbitrary vector changes both its direction and length. (B) Eigenvectors when acted on by a matrix only change their length. The factor by which the length increases is the eigenvalue.

it, that is, changing the direction it is pointing in, and changing its length. A vector for which the action of the matrix leaves the direction it is pointing in unchanged, is called an *eigenvector*. The new vector will still typically have a new length and the ratio of the new to the old length is the *eigenvalue* associated with that particular eigenvector. In order to find the eigenvectors of a matrix, one strategy would be to try all vectors and see which ones remain in the same direction upon action of the matrix. This is clearly not practical since there are too many vectors to try, an infinite number in fact.

To find an eigenvector of a matrix

$$\mathbf{M} = \begin{pmatrix} m_{11} & m_{12} \\ m_{21} & m_{22} \end{pmatrix} \quad (15.58)$$

we need to find the solution to the equation $\mathbf{M}\mathbf{e} = \lambda\mathbf{e}$, which says that the vector \mathbf{e} is the eigenvector of the matrix with eigenvalue λ . Using the rules of matrix multiplication we can expand this matrix equation into a set of two equations with two unknowns:

$$\begin{aligned} m_{11}e_1 + m_{12}e_2 &= \lambda e_1, \\ m_{21}e_1 + m_{22}e_2 &= \lambda e_2. \end{aligned} \quad (15.59)$$

This can be rewritten as

$$\begin{aligned} (m_{11} - \lambda)e_1 + m_{12}e_2 &= 0, \\ m_{21}e_1 + (m_{22} - \lambda)e_2 &= 0, \end{aligned} \quad (15.60)$$

so it takes on the form discussed above, $(\mathbf{M} - \lambda\mathbf{I})\mathbf{e} = 0$, where we have rewritten eqn 15.60 in matrix form using the identity matrix $\mathbf{I} = \begin{pmatrix} 1 & 0 \\ 0 & 1 \end{pmatrix}$. To solve this system of equations we first express e_2 in terms of e_1 from the first of the two equations to obtain

$$e_2 = -\frac{(m_{11} - \lambda)}{m_{12}} e_1, \quad (15.61)$$

where we have assumed that $m_{12} \neq 0$. In case $m_{12} = 0$ we can repeat the same procedure as below by solving the second equation in eqn 15.60 for e_1 . Finally, if both m_{12} and m_{21} are zero then the matrix is diagonal and $\begin{pmatrix} 1 \\ 0 \end{pmatrix}$ and $\begin{pmatrix} 0 \\ 1 \end{pmatrix}$ are its eigenvectors, with m_{11} and m_{22} being the respective eigenvalues.

Next we substitute eqn 15.61 into the second of eqn 15.60, and we arrive at

$$\frac{m_{21}m_{12} - (m_{11} - \lambda)(m_{22} - \lambda)}{m_{12}} e_1 = 0. \quad (15.62)$$

Since we are looking for a nonzero solution to this equation the coefficient in front of e_1 must be zero. In other words,

$$(m_{11} - \lambda)(m_{22} - \lambda) - m_{12}m_{21} = 0 \quad (15.63)$$

needs to hold. This is a quadratic equation whose two solutions λ_1 and λ_2 are the eigenvalues. To get the eigenvectors we can set $e_1 = 1$ and get e_2 from eqn 15.61 using one or the other eigenvalue.

It is important to note the quadratic equation leading to the eigenvalues can also be rewritten in matrix form:

$$\det(\mathbf{M} - \lambda\mathbf{I}) = 0, \quad (15.64)$$

where the operation \det is the determinant of the matrix. In this form the equation for the eigenvalues works for matrices of arbitrary size. For a 2×2 matrix the determinant is the difference between the product of the matrix elements along the two diagonals.

15.2.7 Michaelis–Menten and Enzyme Kinetics

One of the most powerful tools for analyzing biochemical kinetics that exploits rapid pre-equilibrium assumptions like those described in the previous section is the model of Michaelis–Menten kinetics. This simple kinetic scheme will arise in our thinking about cytoskeletal polymerization and molecular motors, and has also been applied to many different kinds of enzymes involved in a wide variety of biological processes ranging from central metabolism to signaling during embryonic development. The Michaelis–Menten framework for thinking about enzyme kinetics offers the power of a unifying approximate description for the huge variety of biological catalysts that use many different detailed mechanisms to perform a wide range of transformations on a plethora of substrates. Within this unifying framework, every enzyme can be approximately characterized by just two parameters: one rate constant describing the maximum turnover rate at which the enzyme can operate if its substrate is present at saturating concentrations, and a second constant describing the magnitude of the substrate concentration required for the enzyme to operate at half its maximal rate. Although the Michaelis–Menten scheme is clearly oversimplified for dealing with the true kinetic complexity of biological enzyme mechanisms, its great simplicity and broad applicability have earned it a central place of honor in the history of biochemistry. Many biochemistry reference books include large tables comparing the activity of different enzymes as characterized by the two quantitative parameters derived from this scheme.

The essential idea in the Michaelis–Menten scheme is that the reaction catalyzed by a given enzyme is composed of two separable steps. The first step (assumed to be readily reversible) involves the formation of an intermediate complex of enzyme and substrate. Once this first step has taken place, the complex can undergo a second reaction resulting in the formation of the product. There are a host of cases in which this kind of thinking is appropriate: (i) promoter occupancy by RNA polymerase is often much faster than escape to form transcripts, (ii) binding of tRNA in the ribosome can be much faster than peptide bond formation, (iii) ATP binding to an enzyme can be much faster than the hydrolysis step, etc.

This class of reactions can be written as



We assume that the final step is irreversible and characterized by the rate constant r . This equation is similar in structure to eqn 15.43 with the important addition of the enzyme E as a catalyst. Note that the enzyme is regenerated after the reaction is complete so that it can go on to catalyze the same reaction for a new substrate molecule.

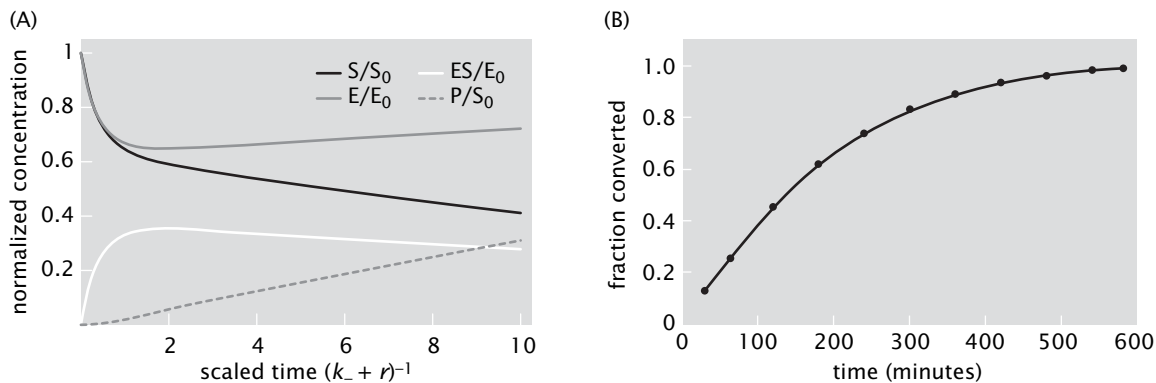


Figure 15.16 Concentrations of reactants and products in an enzyme catalyzed reaction. (A) The graph shows the time evolution of $[E]$, $[S]$, $[ES]$ and $[P]$. Time is defined in units of $1/(k_- + r)$ and $r/(r + k_-) = 0.1$. (B) Experimental data showing the amount of product as a function of time for the hydrolysis of sucrose as catalyzed by the yeast enzyme invertase. At early time points, the function showing product over time is nearly linear as illustrated in (A). At later time points (after about 100 min) the rate of reaction slows down because the substrate is being depleted. (Data adapted from A. J. Brown, *J. Chem. Soc. Trans.*, 81:373, 1902.)

Given this reaction scheme, we can write the rate equations using the rules described earlier in the chapter, resulting in

$$\begin{aligned} \frac{d[E]}{dt} &= -k_+[E][S] + k_-[ES] + r[ES], \\ \frac{d[S]}{dt} &= -k_+[E][S] + k_-[ES], \\ \frac{d[ES]}{dt} &= k_+[E][S] - (k_- + r)[ES], \\ \frac{d[P]}{dt} &= r[ES]. \end{aligned} \quad (15.66)$$

One simple and immediate approach to these equations is to solve them numerically. That is, by starting with some set of initial conditions (that is, $[E]_0$, $[S]_0$, $[ES]_0$ and $[P]_0$ – we use the subscript “0” to signify initial values), we can perform an integration of these dynamical equations to find the resulting time history for the concentrations of all four species. A choice of initial concentrations that illustrates the essence of the dynamics is $[E]_0 = [S]_0 = (k_- + r)/k_+$ and $[ES]_0 = [P]_0 = 0$. In this case, we start out with no intermediate or product. The time evolution of the system in this case is shown in Figure 15.16. Note that the concentration of enzyme initially decreases, but ultimately starts to climb again once the available substrate starts to become too depleted. The reader is invited to explore this analysis in detail in the problems at the end of the chapter.

Of course, often it is of great interest to have an approximate analytic description of a given model for the purposes of developing intuition. The dynamical equations given above can be solved approximately by recourse to certain simplifying assumptions. One powerful scheme is to assume that the intermediate is in steady state corresponding to $d[ES]/dt = 0$. This approximation is reasonable during the relatively early part of the reaction time series where the rate of change of product is approximately linear with time, that is, each enzyme molecule is working at a nearly constant rate. If we make this assumption, then we can obtain the concentration $[ES]$ in terms of $[E]$ and $[S]$ as

$$\frac{[E][S]}{[ES]} = \frac{k_- + r}{k_+} = K_m, \quad (15.67)$$

where we have introduced a new constant, K_m , usually called the Michaelis constant. The value K_m can be intuitively understood as the concentration of substrate where the reaction is proceeding at half the maximum possible rate. If $r \ll k_-$, then K_m is approximately equal

to k_-/k_+ , that is, the dissociation constant K_d for the binding of the substrate to its enzyme.

Our interest is in the rate of product formation under steady-state conditions. We can rewrite the equation for $d[P]/dt$ as

$$\frac{d[P]}{dt} = r \frac{[E][S]}{K_m}. \quad (15.68)$$

This equation can be conveniently rewritten by virtue of the realization that the *maximum* rate of reaction corresponds to $V_{max} = r[E_{tot}]$, which assumes that the entirety of the stockpile of enzyme is bound to substrate and ready to form product. This will be the case when the concentration of substrate is extremely high relative to K_m . Using this definition, we can now rewrite eqn 15.68 as

$$\frac{d[P]}{dt} = V_{max} \frac{[E][S]/K_m}{[E_{tot}]}. \quad (15.69)$$

If we now invoke the fact that $[E_{tot}] = [E] + [ES]$ and use $[ES] = [E][S]/K_m$, we obtain the Michaelis–Menten result,

$$\frac{d[P]}{dt} = V_{max} \frac{[S]/K_m}{1 + ([S]/K_m)}, \quad (15.70)$$

which permits us to compute the rate of reaction as a function of substrate concentration.

The most important conclusion of this analysis for our purposes is that the *rate* of the reaction is going to depend on the concentration of substrate in a very systematic way which is recognized as having the same functional form as the binding curves introduced in Chapter 6. The functional form is plotted in Figure 15.17(A), where it can be seen that K_m corresponds to the substrate concentration needed to reach half maximum velocity. The excellent fit of the curve to experimental data for ATP hydrolysis by the motor protein myosin is shown in Figure 15.17(B).

Although this framework has proved valuable as a basis for thinking about how reaction rates depend upon substrate concentration for almost 100 years, for many real enzymes this analysis is too simplified to be quantitatively faithful to the data, particularly when enzyme rates are measured over a very large range of substrate concentrations. In many cases, the simple Michaelis–Menten kinetics is not applicable because the enzyme–substrate complex must proceed through multiple intermediate steps prior to releasing product. Further complications may arise when an enzyme uses two or more substrate molecules, which may bind to the active site cooperatively, and when enzymes are

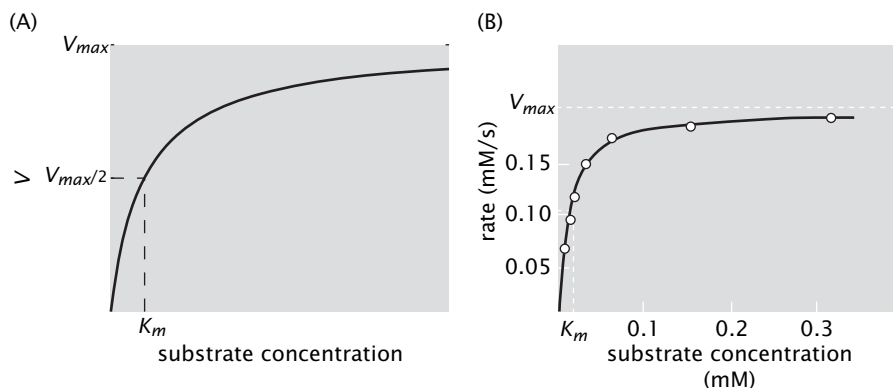


Figure 15.17 Michaelis–Menten kinetics. (A) The general form of the Michaelis–Menten equation showing the enzyme rate as a function of substrate concentration can be captured by just two parameters: the maximal rate for saturating substrate concentrations (V_{max}), and the substrate concentration at which the rate is half of the maximum (K_m). (B) Experimental data showing the rate of ATP hydrolysis by rabbit skeletal muscle myosin as a function of ATP concentration. (B, adapted from L. Ouellette et al., *Arch. Biochem. Biophys.*, 39:37, 1952.)

allosterically activated by regulators that bind at locations other than the active site. In addition, experimental factors often complicate the analysis. For example, product molecules often act as inhibitors for their enzymes so the effective enzyme concentration decreases over time. The reader is invited to explore these questions further both in the problems and in the “Further Reading” at the end of the chapter.

15.3 THE CYTOSKELETON IS ALWAYS UNDER CONSTRUCTION

So far, this chapter has emphasized rate equations as a conceptual framework for treating problems involving the time evolution of reactants and products in chemical reactions. These ideas can be used in a powerful way to explore the dynamics of the cytoskeleton. As a result, we review some of the key examples of cytoskeletal dynamics, and then illustrate how to use the rate-equation paradigm to consider these examples.

15.3.1 The Eukaryotic Cytoskeleton

The Cytoskeleton Is a Dynamical Structure That Is Always Under Construction

The eukaryotic cytoskeleton in mammalian cells is built around three main molecular actors, namely, actin, microtubules, and intermediate filaments as already introduced in Section 10.5.1 (p. 000). One of the most intriguing features of these biological polymers is the fact that they exhibit rich dynamical behavior whether examined *in vitro* or within cells. Indeed, there is a wide variety of cellular processes that depend upon this rich behavior of cytoskeletal filaments. For example, Figure 15.18 shows the way in which microtubules play a role in segregating chromosomes. Similarly, in Figures 15.2 and 15.3, we saw how actin assembly mediates cell motility. The main lesson of these observations is that the cytoskeleton is a constantly changing network that is subject to precise control which dictates when and where filaments will nucleate, attach, branch, and grow.

Though spectacular cellular events like those shown in Figure 15.18 reveal the intricacy of cytoskeletal dynamics, to begin our thinking on model building of such dynamics we begin with the more tractable *in-vitro* situation shown in Figure 15.19. The main idea of the experiments that such cartoons depict is that actin monomers in solution spontaneously aggregate to form filaments. Such experiments were indicated schematically in Figure 15.1(A). One way to perform these measurements is to attach a small molecule covalently to a specific site on actin which is poorly fluorescent when the actin is in its soluble monomeric form, but whose fluorescence is strongly increased once the actin monomers are part of a filament. By monitoring the fluorescence as a function of time, it is possible to measure the rate at which filaments nucleate and grow. Data of this kind are shown in Figure 15.19(C).

As shown in Figure 15.19(A), if actin monomers are placed in solution, after some initial lag time they will nucleate filaments which will then grow until an equilibrium is reached where the rates of detachment and attachment are equal. By way of contrast, as shown in Figure 15.19(B), if the solution is seeded with preexisting nuclei, the growth phase starts immediately and is characterized by the same growth rate. These experiments provide a first clue as to how the cell might control when and

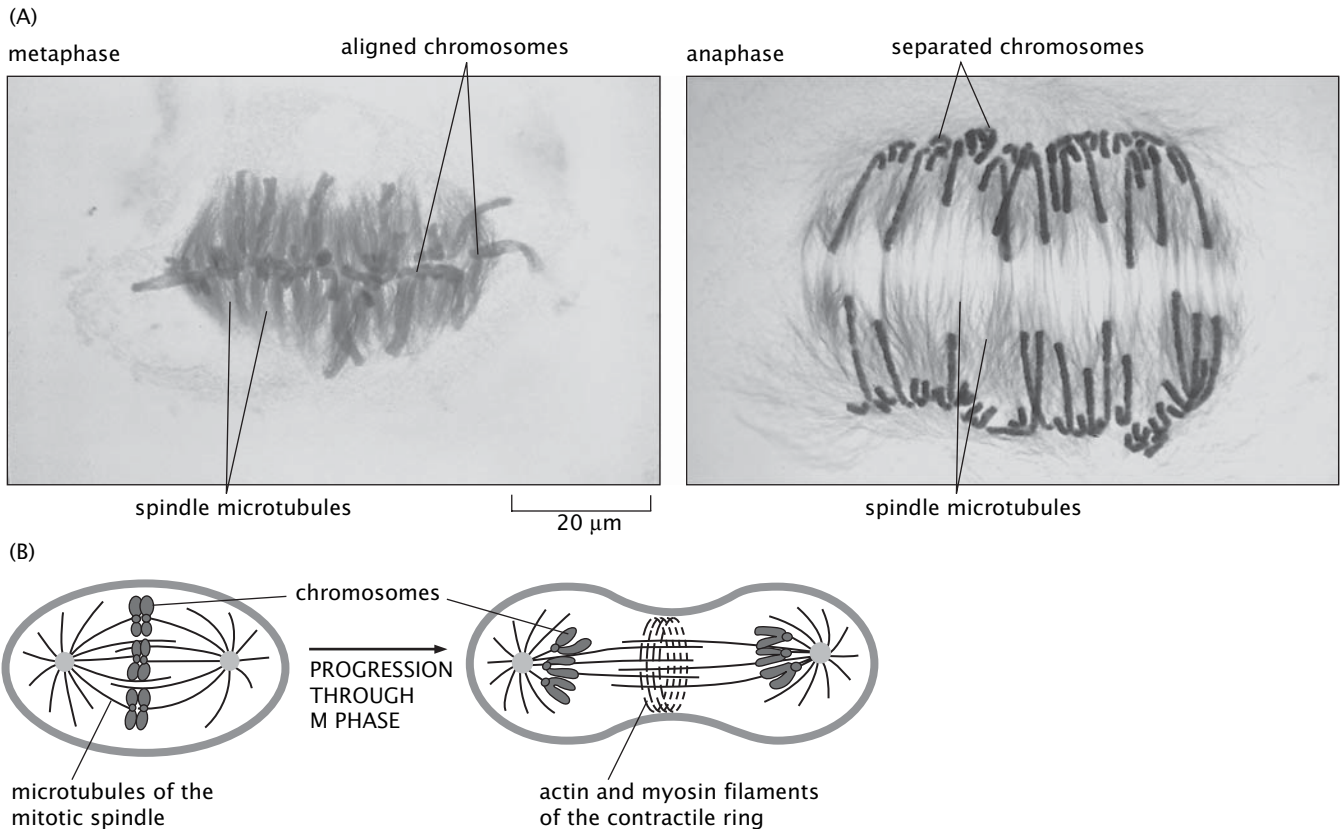


Figure 15.18 Chromosome segregation by microtubules. (A) Micrographs of the transition from metaphase (where the duplicated sister chromosomes are all aligned) to anaphase (where the chromosomes have been separated into two groups) in endosperm cells from a lily. The tubulin is labeled by gold-labeled antibodies. (B) Cartoon showing how microtubules separate the chromosomes and an actin filament ring forms in the middle of the mother cell to split it into two daughters. (A, courtesy of A. Bajer; B, adapted from B. Alberts et al., *Molecular Biology of the Cell*, 5th ed. New York: Garland Science, 2008.)

where filaments are present by tuning their nucleation. Indeed, hundreds of different kinds of actin-associated proteins inside living cells are able to modulate every aspect of actin filament dynamics including the nucleation rate, elongation rate, dissociation rate, ATP exchange rate, large scale architecture, etc. The concentrations of some of these actin-modulating proteins have been determined by experiments such as those shown in Figure 15.4. Actual actin polymerization data showing the effects of such proteins are shown in Figure 15.19(C).

15.3.2 The Curious Case of the Bacterial Cytoskeleton

Historically, it was thought that one of the defining distinctions between bacteria and eukaryotes was that bacteria lacked a cytoskeleton. However, this picture has now changed dramatically with tubulin and actin homologs having been identified in bacteria and possibly an intermediate filament-like protein as well. One example is that of ParM, a bacterial homolog of eukaryotic actin, which is responsible for segregating plasmids upon cell division. In particular, ParM was discovered on a plasmid carrying antibiotic resistance genes that were associated with an outbreak of epidemic typhoid in Mexico and southwestern USA. ParM and its molecular partners are responsible for making sure that in those bacteria that carry the plasmid both daughter cells receive a copy. A schematic of the mechanism of ParM is shown in Figure 15.20.

ParM is an intriguing example since in some ways it can be thought of as a simple version of a mitotic spindle. In Figure 15.18 we showed a picture of a mitotic spindle in action where it is seen how microtubules separate the chromosomes and an actin filament ring forms in the middle of the mother cell. Figure 15.20 elaborates that analogy by depicting the way in which ParM carries out similar functions in the prokaryotic

setting. The basic idea is that the ParM filaments grow and shrink spontaneously until both ends successfully encounter one of the two copies of the antibiotic resistance plasmid. When both plasmids are attached to the different extremities, the filaments polymerize without shrinkage, effectively pushing their plasmid cargo to opposite poles of the dividing cell. Images from a video microscopy sequence of plasmid segregation are shown in Figure 15.20(B).

Other examples of bacterial cytoskeletal homologs are MreB, an actin homolog which is related to genome position and cell shape in some bacteria, and FtsZ, which is a tubulin homolog and one of the main players in the formation of the ring that dictates the plane of cell division. One of the peculiar features of these prokaryotic cytoskeletal proteins is that there is a role reversal relative to their eukaryotic counterparts

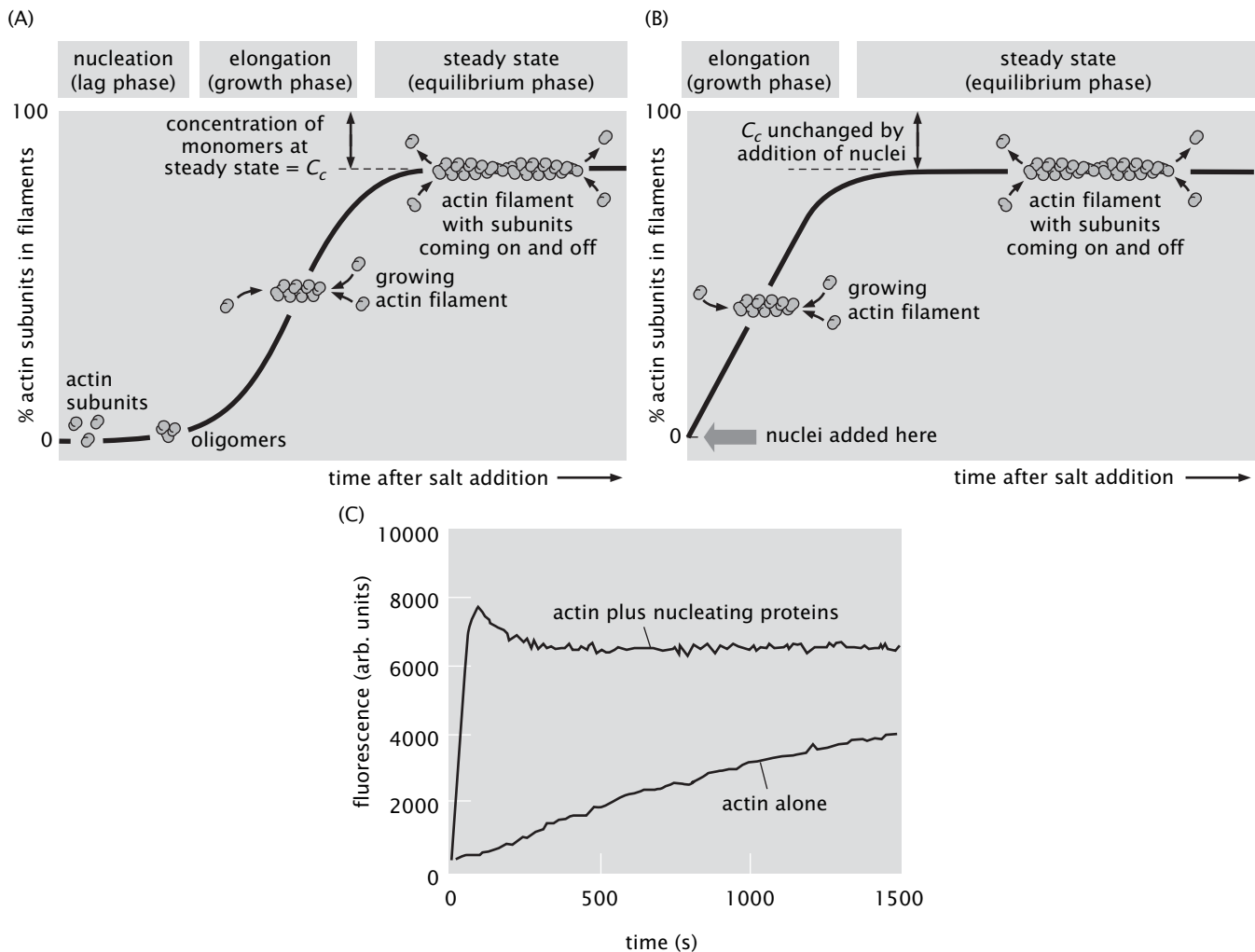


Figure 15.19 Schematic of the rate of polymerization as a function of time. (A) Starting from a pure solution of actin subunits the limiting step in filament assembly is the random collision of at least three subunits to form a nucleus which can then be rapidly elongated. Because nucleus formation is slow compared to filament elongation, a measurement of the total amount of actin in filament form as a function of time will show an initial lag phase. When polymerization is complete, there remains a small amount of actin in solution; this concentration of leftover monomers is called the critical concentration. (B) If stabilized nuclei are added at the beginning of the polymerization reaction, elongation will start immediately and there is no lag phase. The critical concentration is not affected. (C) Experimental growth curves for actin with and without the activity of proteins (Arp2/3 and ActA) that nucleate filaments. The slow growth case corresponds to no Arp2/3. (A, B, adapted from B. Alberts et al., *Molecular Biology of the Cell*, 5th ed. New York: Garland Science, 2008; C, adapted from M. D. Welch et al., *Science*, 281:105, 1988.)

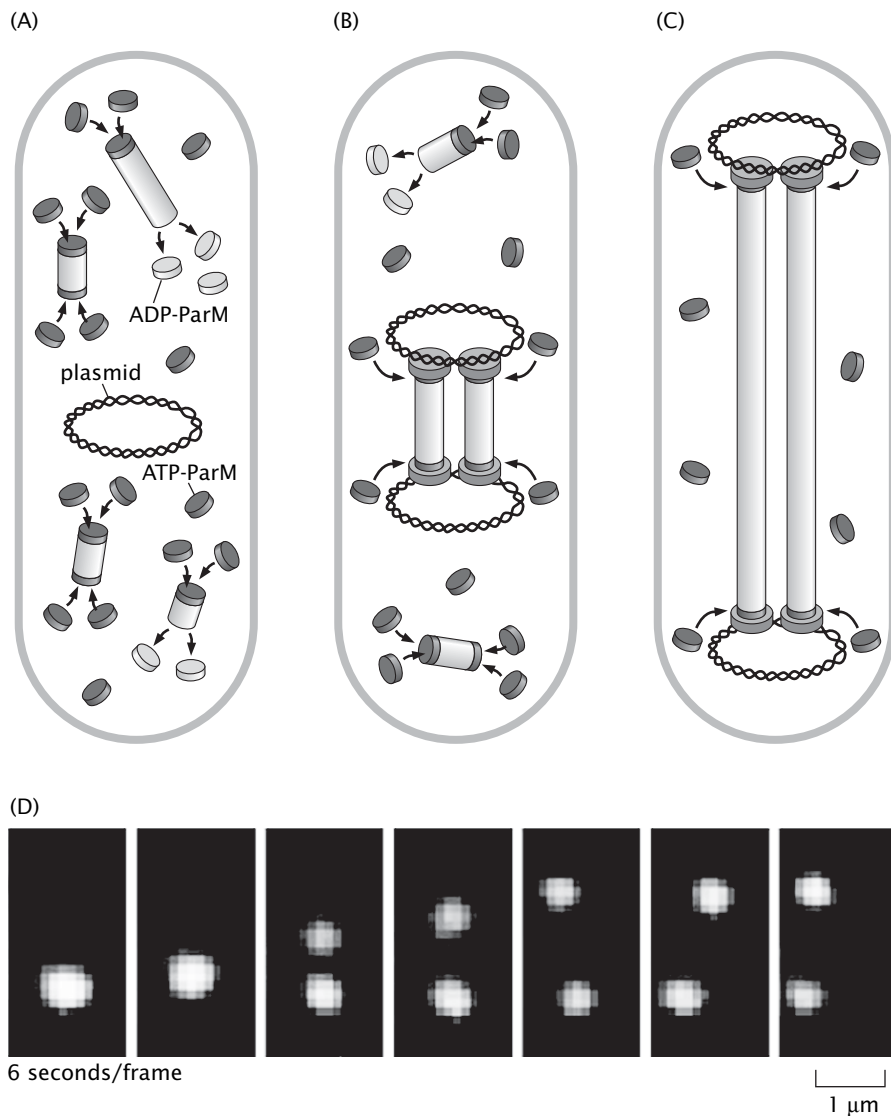


Figure 15.20 A model for plasmid segregation driven by the bacterial actin homolog ParM. (A) Some bacterial plasmids carry antibiotic resistance genes that are found at very low copy numbers inside cells, as few as 1–2 per cell. In order to maintain their presence in the bacterial population, these plasmids require a mechanism for segregation analogous to the mechanisms for chromosome segregation. The R1 plasmid encodes an actin homolog ParM which is continuously expressed. ParM filaments are extremely unstable. (B) After the plasmid has replicated, unstable ParM filaments can be stabilized when their two ends come into contact with specific sites on the two plasmids. The filaments can continue to elongate at the site of DNA binding. (C) The insertional elongation of ParM filaments pushes the two copies of the plasmid to opposite poles of the cell. (D) Time lapse sequence showing segregation of two fluorescently tagged plasmids in a living *E. coli* cell. (A–C, adapted from E. C. Garner et al., *Science* 306:1021, 2004; D, adapted from C. S. Campbell and R. D. Mullins, *J. Cell Biol.*, 179:1059, 2007.)

with actin homologs undertaking tasks reserved for microtubules in the eukaryotic setting and vice versa. The study of the cytoskeleton in both prokaryotes and eukaryotes provides an interesting opportunity to put the rate equation ideas developed in this chapter to work.

15.4 SIMPLE MODELS OF CYTOSKELETAL POLYMERIZATION

Huge classes of cellular processes can ultimately be thought of in terms of the addition of monomers to the ends of growing chains: transcription and translation, cytoskeletal assembly, polymerization of filamentous viruses such as tobacco mosaic virus, etc. The simplest picture of such polymerization reactions amounts to assuming that there is a characteristic rate of addition of monomers to the end of a growing polymer and that there is a characteristic rate at which monomers fall off the end of such polymers. These ideas lead naturally to various classes of dynamic models.

The Dynamics of Polymerization Can Involve Many Distinct Physical and Chemical Effects

For concreteness, we use actin as our first case study. Our plan is to consider a hierarchy of models of increasing complexity as shown in Figure 15.21. The key quantities that we will reason about are the probability distribution $P_n(t)$, which delivers the probability of having a filament of length n at time t , and $\langle L \rangle$, which characterizes the average length of the polymers. The simplest level of approximation for determining these quantities posits polymerization processes in which the on and off rates at the two ends of the growing polymer are the same and there are no associated nucleotide hydrolysis reactions. The next level in our hierarchy of models asserts a difference in the on and off rates on the two ends of the filament. However, what makes biological polymers like actin and microtubules so intriguing is the fact that they are ATPases (or GTPases), which means that nucleotide hydrolysis reactions are a central part of their dynamics, and as a result of these hydrolysis

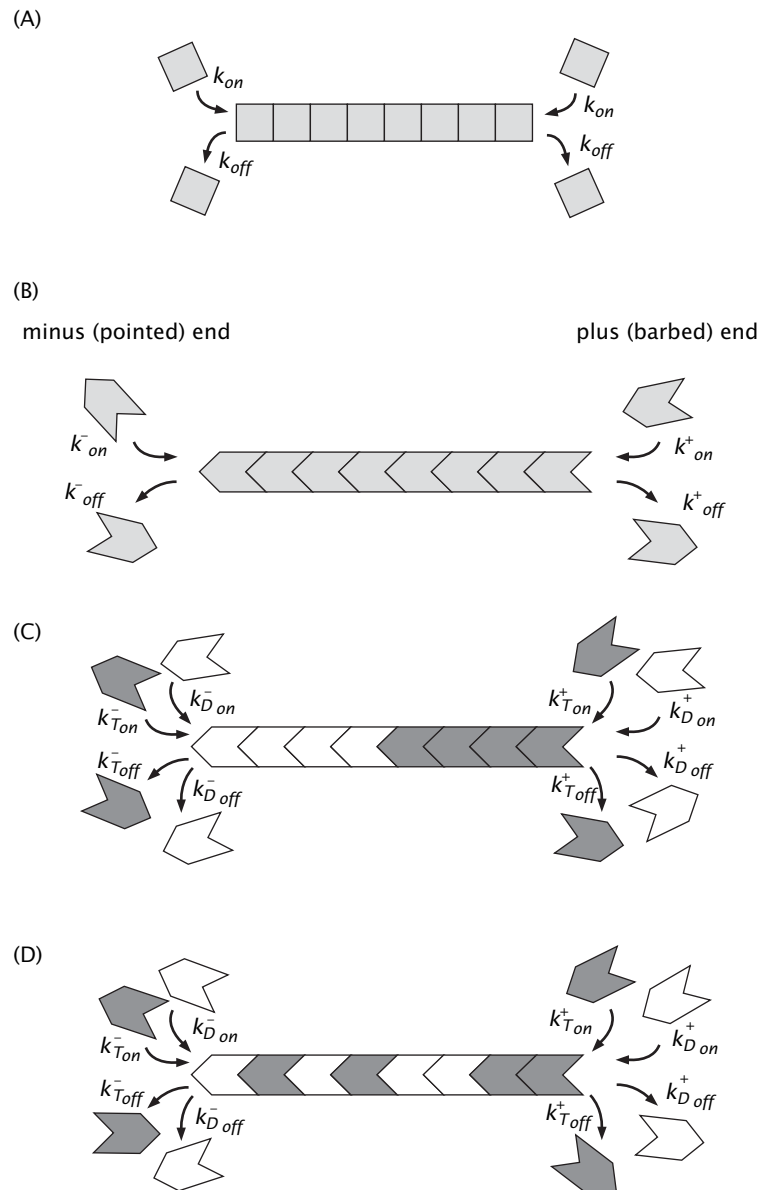
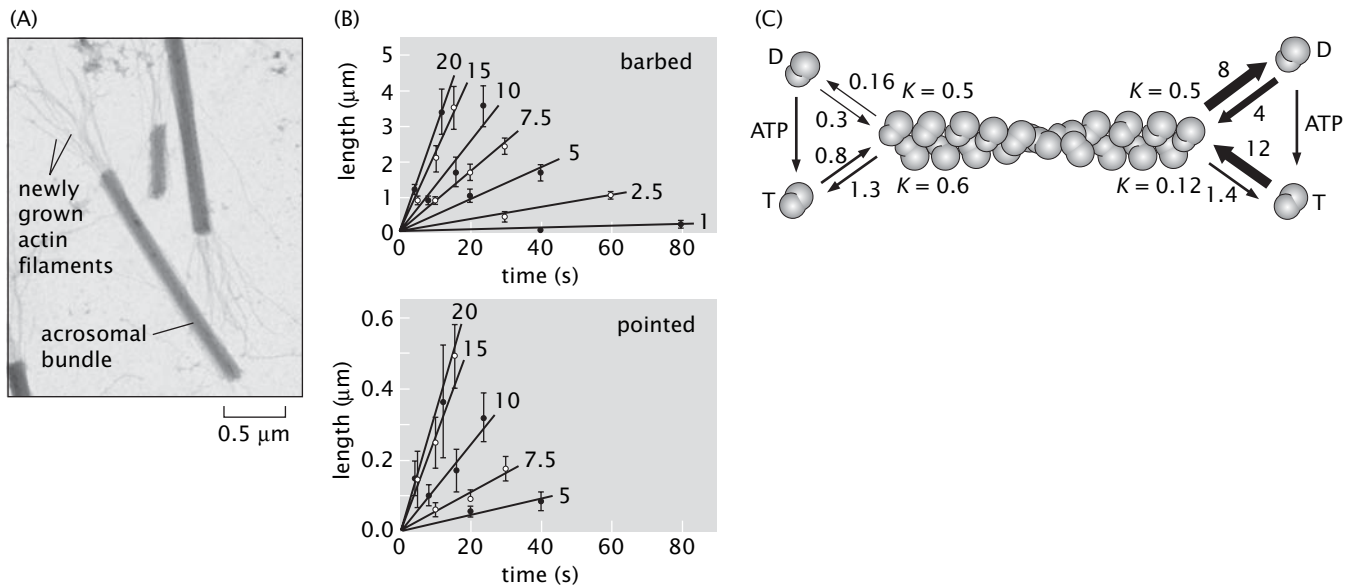


Figure 15.21 Hierarchy of models of cytoskeletal polymerization which include features such as asymmetric rates and hydrolysis. (A) Polymerization with equal rates on both ends. (B) Polymerization with unequal rates on the two ends due to structural asymmetry of the filament. The two structurally distinct ends are often called the plus and minus ends or, for actin, the barbed and pointed ends. (C) Polymerization with unequal rates and vectorial hydrolysis reaction of nucleotides on incorporated monomers. (D) Polymerization with hydrolysis that can take place on any monomer within the filament. For each case, the rate constants are illustrated. Different rate constants may apply for on rates and off rates, plus and minus ends of filaments and ATP vs ADP containing subunits.



reactions, the system can behave more creatively with respect to on and off rates on the two ends. Figure 15.22 gives a quantitative picture of the actin polymerization process when the full asymmetry and hydrolysis rates are included.

15.4.1 The Equilibrium Polymer

Equilibrium Models of Cytoskeletal Filaments Describe the Distribution of Polymer Lengths for Simple Polymers

The simplest model that one might try in thinking about biological polymers is an equilibrium model in which the dynamics results from statistical fluctuations at the two ends. Such models provide a useful description of the formation of biological filaments such as bacterial flagella, filamentous viruses, and amyloid protein fibers. At the same time, such models lack the nuance to capture some of the most intriguing dynamical features of cytoskeletal polymers (actin, microtubules, and their bacterial homologs) such as treadmilling and dynamic instability. One of the first classes of data that such a model can confront is the distribution of filament lengths such as is shown in Figure 15.23. In particular, this figure shows a histogram of the distribution of filament lengths and effectively counts up how many filaments of each length are found.

Our starting point for the equilibrium analysis is the assertion that the probability distribution for the different lengths is stationary, which implies $dP_n/dt = 0$. In this case, the equilibrium is characterized by

$$P_n + P_1 \xrightleftharpoons{K_d} P_{n+1}, \quad (15.71)$$

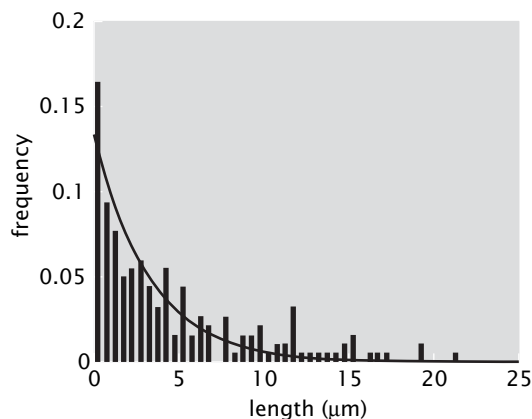
which can also be written in a more useful form as

$$K_d = \frac{[P_n][P_1]}{[P_{n+1}]}. \quad (15.72)$$

In principle, K_d should be a function of n since the reaction of two monomers to form a dimer is not necessarily the same as the reaction of a 1000-mer and a monomer to form a 1001-mer. For simplicity, we make the extra assumption that K_d does not depend upon the number

Figure 15.22 Rates of actin polymerization. (A) Electron micrograph showing polarized growth of actin filaments from the ends of horseshoe crab sperm acrosomal bundles. These bundles consist of a parallel array of stabilized actin filaments. When monomeric actin is added it will form new filaments at different rates on the barbed end and on the pointed ends of the acrosome. Here tufts of long filaments can be seen growing from the barbed ends of several acrosomal bundles. (B) Length as a function of time for actin growth from barbed and pointed ends of acrosomal bundles. The actin monomer concentration in μM is shown next to each time course. Note the difference in scales; barbed end growth is approximately 10 times faster than pointed end growth. (C) Cartoon of G-actin polymerization. On rates are given in $(\mu\text{M s})^{-1}$, off rates in s^{-1} and dissociation constants in μM . (A, courtesy of M. Footer; B, C, adapted from T. D. Pollard, *J. Cell Biol.*, 103:2747, 1986.)

Figure 15.23 Distribution of filament lengths for actin filaments. (Adapted from S. Burlacu et al., *Am. J. Physiol.*, 262:C569, 1992.)



of monomers. If we consider the case when $n = 1$ in eqn 15.72 we find

$$K_d = \frac{[P_1][P_1]}{[P_2]} = \frac{[P_1]^2}{[P_2]} \Rightarrow [P_2] = \frac{[P_1]^2}{K_d}. \quad (15.73)$$

We can adopt the same strategy again by taking $n = 2$ and use the result from the previous iteration to find

$$K_d = \frac{[P_2][P_1]}{[P_3]} = \frac{[P_1]}{[P_3]} \cdot \frac{[P_1]^2}{K_d} \Rightarrow [P_3] = \frac{[P_1]^3}{K_d^2}. \quad (15.74)$$

By inspection, we can now write the general result as

$$[P_n] = \frac{[P_1]^n}{K_d^{n-1}} = K_d \left(\frac{[P_1]}{K_d} \right)^n. \quad (15.75)$$

This result now permits us to examine the equilibrium distribution of lengths of simple polymers. In particular, it provides a basis for estimating the number of 2-mers, 3-mers and so on. We can rewrite eqn 15.75 in a friendlier way as

$$[P_n] = K_d e^{n \ln([P_1]/K_d)} = K_d e^{n \ln([P_1]/K_d)} = K_d e^{-\alpha n}, \quad (15.76)$$

where we define $\alpha = -\ln([P_1]/K_d)$. For the case in which $[P_1] < K_d$, we see immediately that the distribution is a decreasing function of the length as is revealed in Figure 15.23.

Given the distribution of polymer lengths in this simple equilibrium model, we are now poised to compute the average length of these filaments. In particular, the calculation of interest is

$$\langle n \rangle = \frac{\int_0^{\infty} n e^{-\alpha n} dn}{\int_0^{\infty} e^{-\alpha n} dn} = \frac{1}{\alpha} = \frac{1}{\ln(K_d/[P_1])}. \quad (15.77)$$

Using the value of K_d determined above we can plot the average length as a function of the monomer concentration as shown in Figure 15.24. The average length is a very sensitive function of the monomer concentration. As a result, if the cell were to exploit an equilibrium mechanism of this form it would necessarily involve very fine tuning of monomer concentrations. In reality, some polymers that polymerize using this mechanism have other means for determining their preferred length. For example, filamentous viruses such as the tobacco mosaic virus (TMV) use their nucleic acid genome as a template to decide how long to grow. To get a better feeling for the implications of this model, we can also examine the nature of the fluctuations it predicts.

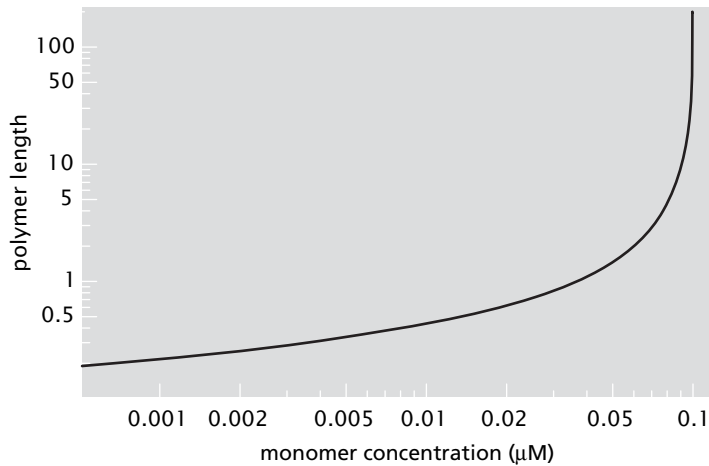


Figure 15.24 Average length of the filaments as a function of the monomer concentration for the equilibrium model.

Estimate: Equilibrium Polymers? In order to see what this simple equilibrium model of biological polymers has to say, we require an estimate of K_d . One way that we can obtain an estimate of K_d is as the ratio k_{off}/k_{on} . By appealing to the known rates for actin and ignoring the fact that these rates depend upon whether the monomers are bound to ATP or ADP, we have $k_{on} \simeq 10 \mu\text{M}^{-1}\text{s}^{-1}$ and $k_{off} \simeq 1\text{s}^{-1}$. Using these numbers we find $K_d = k_{off}/k_{on} \simeq 0.1 \mu\text{M}$. For self-assembling polymers, the K_d is also often referred to as the critical concentration (c^*). Starting with a solution of monomers, if the concentration is above c^* , then filaments will form, but below c^* they will not. As usual, we find it useful to convert concentrations to mean spacings. In this case, this concentration corresponds to a mean spacing of roughly 200 nm. Recall that the size of the individual monomers is on the order of 5 nm, and the mean spacing between macromolecules in a typical cell is less than 10 nm. The fact that monomers can find each other and rapidly form filaments over such large intermolecular spacings emphasizes the importance of rapid diffusive motion.



ESTIMATE

An Equilibrium Polymer Fluctuates in Time

The fact that a system is in equilibrium does *not* mean that it is static. As already illustrated in the case of Brownian motion, systems that are in equilibrium undergo diffusive fluctuations. We can borrow this kind of thinking to examine how the length of an equilibrium polymer will vary in time as a result of the growth and shrinkage of filaments due to their natural fluctuations. In particular, we ask the question: how long do we have to wait for the length to change by $1 \mu\text{m}$ due to these fluctuations? The model we examine is shown schematically in Figure 15.25.

To examine the dynamics of an equilibrium filament we discretize time into steps of length Δt . At every instant, as shown in Figure 15.26, there are three possible fates at both ends of the filament: the end can remain unchanged, the end can lose a monomer, or the end can take on another monomer. With the trajectories and weights in hand, we can work out the average dynamical excursion of the system by summing over all microtrajectories of the system with each one appropriately weighted by the statistical weight. Within this framework, the probability of growth by an amount a (the length of a monomer) is given

Figure 15.25 Cartoon of a filament growing and shrinking by fluctuations. At $t = 0$, the length of the filament is slightly larger than the mean length. Over time, the two ends are subject to fluctuations as monomers are added and removed from both ends.

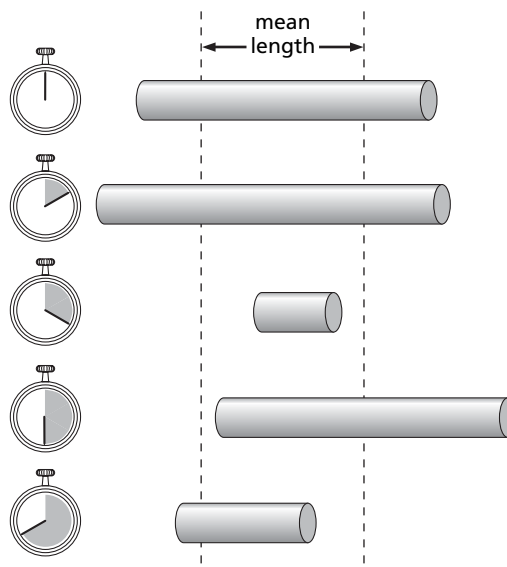
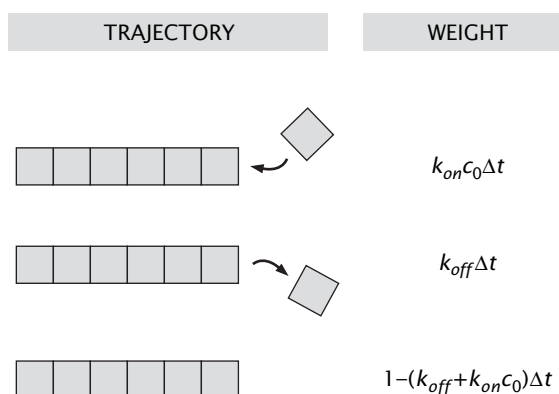


Figure 15.26 Trajectories and weights for an equilibrium polymer. The schematic shows the three processes that are available to a polymer at every time step.



by

$$P(a) = k_{on}c_0\Delta t, \quad (15.78)$$

where c_0 is the concentration of monomers. The probability of shrinkage by a length a is given by

$$P(-a) = k_{off}\Delta t. \quad (15.79)$$

Finally, the probability of nothing happening is

$$P(0) = (1 - k_{on}c_0\Delta t - k_{off}\Delta t). \quad (15.80)$$

Recall that in equilibrium the critical concentration is given by $c^* = k_{off}/k_{on}$, which implies that $P(a) = P(-a)$. As a result, the average change in length in one time step is

$$\underbrace{\langle x \rangle}_{\text{in } \Delta t} = aP(a) - aP(-a) = 0. \quad (15.81)$$

This result is not surprising since effectively, the tip of the filament may be thought of as a random walker that has the same probability of going to the right or to the left. A more telling measure of the fluctuations is

provided by the mean square displacement given by

$$\langle x^2 \rangle = a^2 P(a) + a^2 P(-a) = a^2 k_{on} c_0 \Delta t + a^2 k_{on} c_0 \Delta t = 2a^2 k_{on} c_0 \Delta t. \quad (15.82)$$

We are interested in finding out how many time steps it will take to accumulate a total excursion which is typical of the length change seen in cytoskeletal filaments, such as $1 \mu\text{m}$. Since each instant is independent of the previous instant (that is, there is no memory), the accumulated variance over N steps is N times the variance associated with one step. In particular, we have

$$\langle L^2 \rangle = 2Na^2 k_{off} \Delta t, \quad (15.83)$$

which can be rewritten by noting that $N = t/\Delta t$, resulting in

$$\langle L^2 \rangle = 2a^2 k_{off} t. \quad (15.84)$$

The significance of this result is best served by considering some real-world numbers. Our interest is in the time we have to wait to see an excursion of length L which is given by

$$\sqrt{\langle L^2 \rangle} = \sqrt{2a^2 k_{off} t}. \quad (15.85)$$

For the special case in which we query the time needed for an excursion of length $1 \mu\text{m}$, we have

$$t = \frac{\langle L^2 \rangle}{2a^2 k_{off}}. \quad (15.86)$$

Using the various approximate parameters described above, this yields

$$t = \frac{1 \mu\text{m}^2}{2 \left(\underbrace{\frac{4}{1000} \mu\text{m}}_a \right)^2 1 \text{s}^{-1}} \simeq 9 \text{ hours}. \quad (15.87)$$

The time scales generated by the equilibrium model are clearly inconsistent with the observed time scales of cytoskeletal dynamics. The easiest way to note that is to watch a time-lapse video of a motile or dividing cell and to observe that these processes take place on the minute rather than hour time scales. These rapid dynamics require nucleotide hydrolysis by actin and microtubules and also the activity of myriad other cytoskeleton-associated proteins. The fact that the cytoskeleton is *not* in equilibrium is necessary to give the cell morphological flexibility over rapid time scales. In Section 15.4.3, we will return to the issue of nucleotide hydrolysis by cytoskeletal filaments. In preparation, we first consider the time-dependent behavior of simple nonhydrolyzing polymers.

15.4.2 Rate Equation Description of Cytoskeletal Polymerization

Polymerization Reactions can be described by Rate Equations

Cytoskeletal polymerization consists of three very distinctive phases as shown in Figure 15.19(A). If we start with a situation where we only have monomers free in solution there will be a *lag phase* during which these monomers assemble into small oligomers. After this nucleation

phase and once these nucleation seeds are assembled, the *growth phase* begins. Filament elongation will continue until a *steady state phase* is reached. Here there will still be an interchange of monomers between the solution and the filaments, but the net length change will be zero. In those cases where nuclei are added directly to the solution, the lag phase can be bypassed resulting in growth like that shown in Figure 15.19(B).

As an alternative to the equilibrium model described above and in response to experiments like those indicated schematically in Figure 15.19, we consider the simplest case of a system which is seeded with M “nuclei” which can serve to nucleate growing filaments. Our plan is to write down a rate equation that examines the number of monomers ($n(t)$) associated with the “average” filament at each instant in time. Since our rate equation picture does not consider fluctuations, we note that the dynamical equation describing the number of monomers (n) in each filament is identical for each filament and is given by

$$\frac{dn}{dt} = \underbrace{k_{on} \left(c_0 - \frac{Mn(t)}{V} \right)}_{\text{growth}} - \underbrace{k_{off}}_{\text{shrinkage}}, \quad (15.88)$$

where c_0 is the initial concentration of monomers in the volume V and M is the number of nuclei which seed the growth. This equation says that there will be an addition of monomers with rate k_{on} which is proportional to the monomer concentration. In addition to the growth, there is also the potential of shrinkage of the filaments as a result of the k_{off} term. As the monomer concentration varies, there is a competition between these two terms. The significance of the factor $(c_0 - (Mn/V))$ is that it captures the instantaneous concentration. Our picture is of a box of fixed volume V that has some initial number of monomers c_0V available for polymerization. As the filament growth process proceeds, the number of available monomers is reduced since ever more monomers are now tied up in filaments (the number of monomers in the filaments is Mn) and are hence unavailable for further polymerization. Note that in this simple model, the total number of nuclei (M) is fixed.

The solution to this dynamical equation is found by noting that we have a first-order, linear differential equation which can be rewritten as

$$\frac{dn}{dt} + \frac{k_{on}Mn}{V} = k_{on}c_0 - k_{off}. \quad (15.89)$$

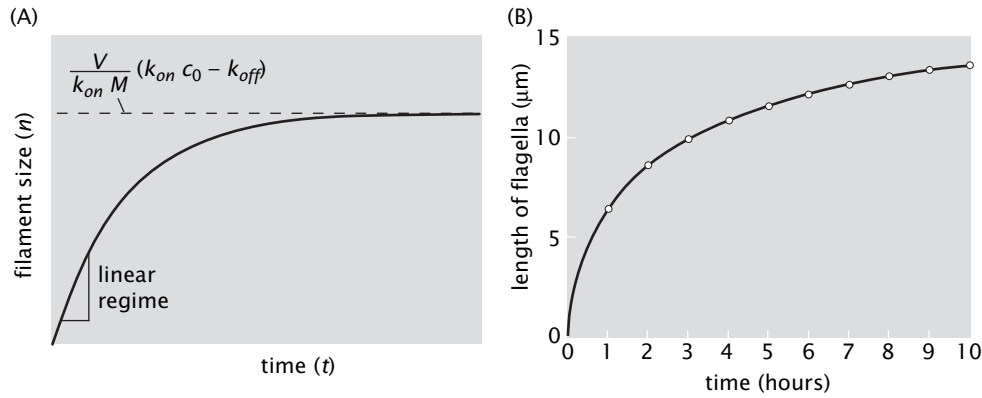
When written in this form, we see that it can be solved by first guessing a “particular” solution, in this case

$$n_{\text{particular}}(t) = \frac{V}{Mk_{on}}(k_{on}c_0 - k_{off}). \quad (15.90)$$

To this particular solution should then be added a solution to the equation for the case in which the right-hand side of eqn 15.89 has been set to zero. The solution in this case is

$$n_{\text{homogeneous}}(t) = Ae^{-k_{on}Mt/V}, \quad (15.91)$$

where the constant A is an arbitrary constant that is fixed by initial conditions. One particular case of interest is the one in which the initial size of the nuclei is zero (of course, this contradicts the idea that a critical nucleus is needed to start the polymerization process, but this choice is mathematically convenient and gives rise to the same key features).



Using $n(0) = 0$ we can fix the constant A as

$$A = -\frac{V}{Mk_{on}}(k_{on}c_0 - k_{off}). \quad (15.92)$$

As a result of these manipulations, the solution to our problem is given by

$$n(t) = \frac{V}{Mk_{on}}(k_{on}c_0 - k_{off})(1 - e^{-k_{on}Mt/V}). \quad (15.93)$$

In order to compute the length of the growing filament, we note that the length is given by

$$L(t) = an(t), \quad (15.94)$$

where a is the length per monomer. This result is plotted in Figure 15.27, which exhibits two key regimes. First, in the short-time limit, defined as times much shorter than the time

$$\tau = \frac{V}{Mk_{on}}, \quad (15.95)$$

the filaments grow linearly with time. This can be seen by considering the behavior at short times which is revealed by expanding $e^{-k_{on}Mt/V}$ in a Taylor series (that is, using $e^x \approx 1 + x$ – see “The Math behind the Models” on p. 000). The second key regime is the long-time limit for which the growth saturates and the length of each filament is constant.

The Time Evolution of the Probability Distribution $P_n(t)$ can be Written Using a Rate Equation

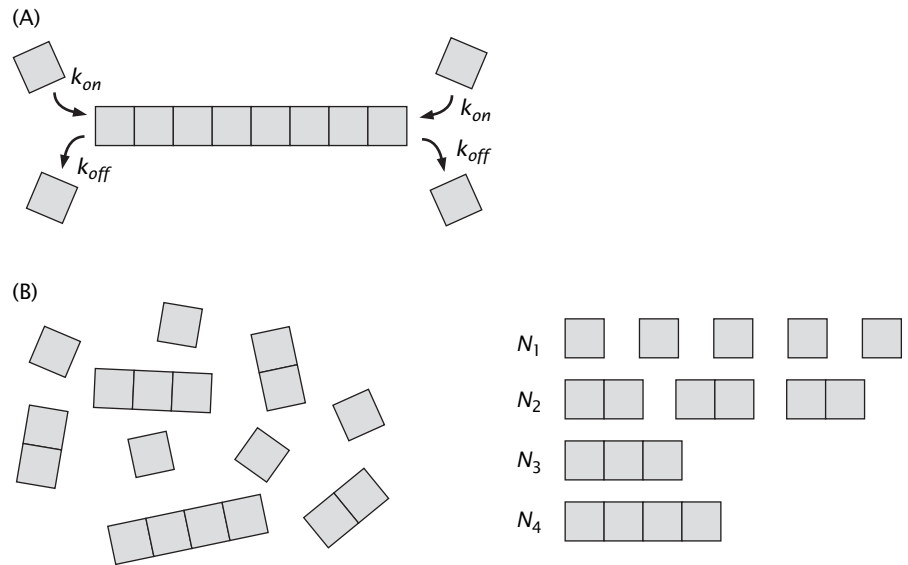
A more sophisticated version of the model we developed above asks for the time evolution of the probability distribution $P_n(t)$, which reflects the probability of finding filaments of length n as a function of time. In particular, $P_n(t)$ is the probability that a given filament is an n -mer and is given as

$$P_n(t) = \frac{N_n}{\sum_{n=1}^{\infty} N_n}, \quad (15.96)$$

where N_n is the number of filaments containing n monomers. Figure 15.28 shows how one takes a distribution of filaments and uses a

Figure 15.27 Average filament size vs time. (A) Length of the filaments as a function of time assuming M initial nuclei. During the initial stages of growth, the growth rate is linear, while at long times the system reaches steady state. (B) Data showing length of filaments vs time for assembly of bacterial flagellin. (B, adapted from T. Iino, *J. Supramol. Struct.*, 2:372, 1974.)

Figure 15.28 Illustration of the idea of the probability distribution $P_n(t)$. (A) The reactions that can change the current length of the filament. (B) A distribution of filaments of various lengths. We count up the number of each species N_1, N_2 , etc.



histogram to determine experimentally the probabilities of the various polymer lengths.

The rate equation that captures the change in the number of n -mers can be written symbolically as

$$\frac{dP_n}{dt} = \text{rate of monomer addition to } n\text{-mer} - \text{rate of monomer removal.} \quad (15.97)$$

To proceed, we make the simplifying assumption that the only way a given n -mer can change its length is by either the addition or loss of a single monomer. For example, we reject the process in which a 5-mer is added to a 4-mer resulting in a 9-mer. In addition, we begin our analysis by assuming that both ends of the growing filament are the same. This assumption will be suppressed later in favor of the experimentally relevant situation in which cytoskeletal filaments have polarity.

The reaction we are proposing is



Our goal is to write a rate equation for the dynamics of this reaction. However, the equations are coupled. That is, the equation for the evolution of P_n depends upon the evolution of both P_{n-1} and P_{n+1} . To find the time evolution of P_n we have to consider the “adjacent” reaction given by



which will account for the “decay” of a polymer of length n into one of length $n - 1$. The time evolution of the probability distribution is governed by four distinct classes of process and is captured mathematically as

$$\frac{dP_n}{dt} = \underbrace{k_{on}P_{n-1}P_1}_{\text{addition to } P_{n-1}} + \underbrace{k_{off}P_{n+1}}_{\text{removal from } P_{n+1}} - \underbrace{k_{on}P_nP_1}_{\text{addition to } P_n} - \underbrace{k_{off}P_n}_{\text{removal from } P_n}. \quad (15.100)$$

One question of immediate interest that emerges from a model of this kind is: what is the average length of a polymer as a function of time whose growth is described by eqn 15.100? If a is the length of a monomer we can write the total average length of the filament as

$$\langle L \rangle = \sum_{n=1}^{\infty} na P_n. \quad (15.101)$$

By taking the time derivative of this expression, we can then write an equation for the time evolution of the average length as

$$\frac{d\langle L \rangle}{dt} = \sum_{n=1}^{\infty} na \frac{dP_n}{dt} \quad (15.102)$$

We can now substitute our expressions for the time derivatives themselves from the original rate equation (eqn 15.100) with the result

$$\frac{d\langle L \rangle}{dt} = \sum_{n=1}^{\infty} na(k_{on}P_{n-1}P_1 + k_{off}P_{n+1} - k_{on}P_nP_1 - k_{off}P_n). \quad (15.103)$$

We may now rearrange the right-hand side resulting in

$$\frac{d\langle L \rangle}{dt} = \sum_{n=1}^{\infty} ank_{on}P_1(P_{n-1} - P_n) + \sum_{n=1}^{\infty} ank_{off}(P_{n+1} - P_n). \quad (15.104)$$

The next step in our argument is to factor out P_1 and to simplify the functional form of the expressions using the identity

$$\sum_{n=1}^{\infty} nP_{n-1} = 2P_1 + 3P_2 + \dots = \sum_{n=1}^{\infty} (n+1)P_n. \quad (15.105)$$

Using this identity several times in our original expression results in

$$\begin{aligned} ak_{on}P_1 \sum_{n=1}^{\infty} n(P_{n-1} - P_n) &= ak_{on}P_1 \sum_{n=1}^{\infty} [(n+1) - n]P_n \\ &= ak_{on}P_1 \sum_{n=1}^{\infty} P_n = ak_{on}P_1. \end{aligned} \quad (15.106)$$

The net result of these manipulations is that we recover precisely the same expression determined earlier for the mean length, namely,

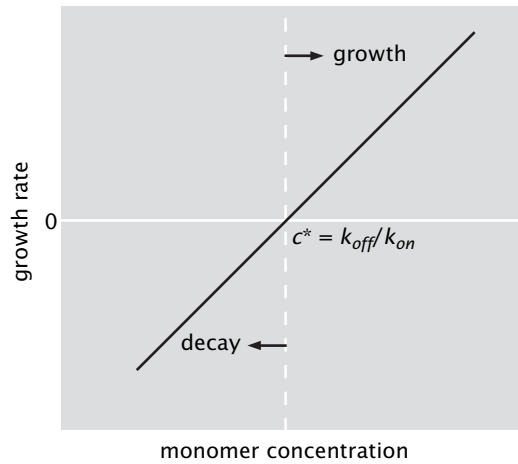
$$\frac{d\langle L \rangle}{dt} = (k_{on}P_1 - k_{off})a. \quad (15.107)$$

One useful way to visualize the significance of this result is to plot the rate of growth as a function of monomer concentration as is shown in Figure 15.29. Note that depending upon the concentration, the filaments will either grow or shrink. In particular, for concentrations smaller than k_{off}/k_{on} the filaments will shrink, whereas for larger values of monomer concentration the filaments will grow. In the special case where P_1 is equal to the critical concentration $c^* = k_{off}/k_{on}$ the average length will not change because $d\langle L \rangle/dt = 0$.

Rates of Addition and Removal of Monomers Are Often Different on the Two Ends of Cytoskeletal Filaments

As was already hinted at in Figure 15.21, there is a hierarchy of models of biological polymerization reactions of increasing physical realism.

Figure 15.29 Growth rate for filaments. The graph shows the growth rate as a function of the monomer concentration. Below a critical concentration, filaments shrink. For concentrations greater than the critical concentration, the filaments grow.



The next refinement of the models we have considered thus far which brings us one step closer to the behavior of real cytoskeletal filaments is to consider the case in which the rates on the two ends of the growing filament are different. The schematic depiction of this situation is shown in Figure 15.30 and reflects the idea that this difference in rates on the two ends is a result of structural asymmetry on the two ends. Stated differently, cytoskeletal polymers such as actin are characterized by a polarity with the distinct ends being labelled as “plus” and “minus” (for historical reasons the plus end on actin is also called the barbed end and the minus end is called the pointed end). As shown in Figure 15.30, the plus end has a faster growth rate than the minus end, and also a faster shrinkage rate.

One intriguing feature of this model is that the ratios of the rates on the two ends must equal each other. The simplest way to see this is to note that the molecular interfaces at the two ends are identical and hence they imply the same free energy associated with the contacts.

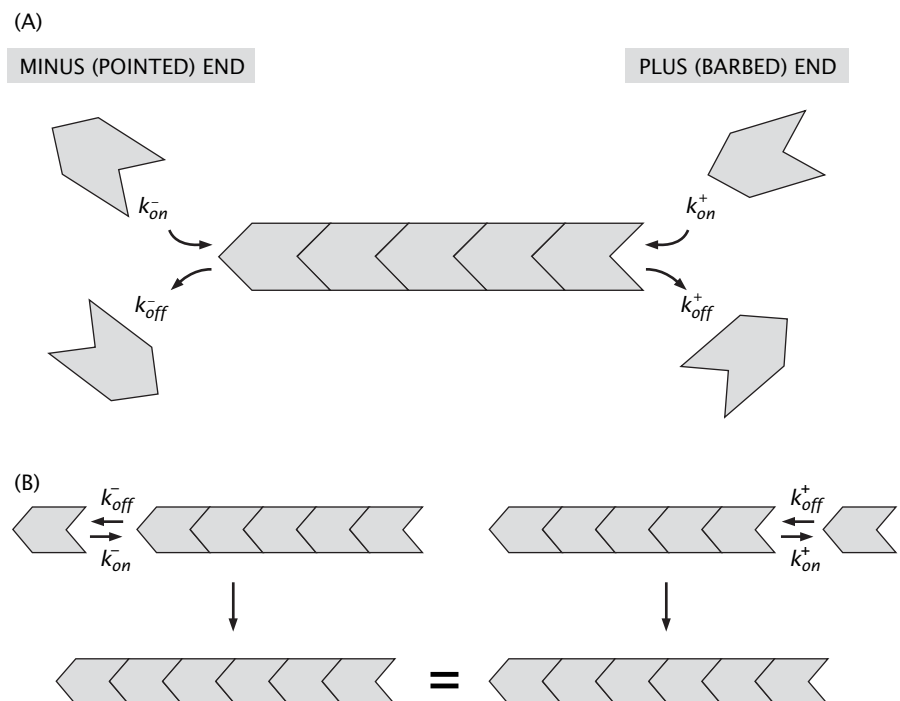


Figure 15.30 Model of polymerization where each end has its own rates. (A) Illustration of the different rate constants on the barbed and pointed ends. (B) Addition of a single monomer to the growing filament.

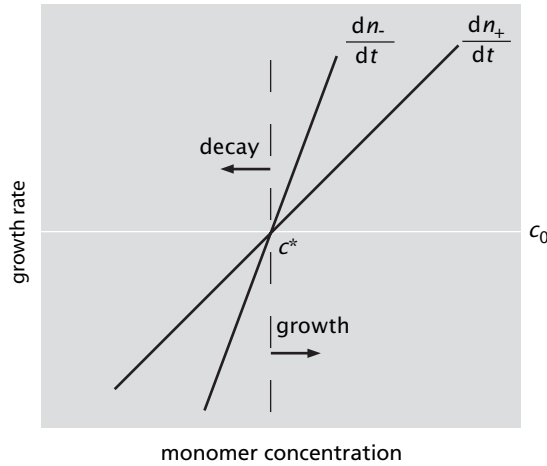


Figure 15.31 Growth rate for the case where the rates for each end of the filament are different. Above the critical concentration (c^*), both ends grow and below the critical concentration, both ends shrink.

Inspection of the schematic in Figure 15.30(A) reveals that although the monomers are themselves asymmetric, once two of them have joined together, the common interface they share is indifferent to whether the monomer was added on the plus or minus end. This condition is represented mathematically as

$$\Delta G^+ = \Delta G^- \Rightarrow \frac{k_{off}^+}{k_{on}^+} = \frac{k_{off}^-}{k_{on}^-} = \frac{1}{V} e^{\Delta G/k_B T}. \quad (15.108)$$

The rate equations for this situation are identical in form on the two ends, though characterized by different rates, and are given by

$$\frac{dn_+}{dt} = k_{on}^+ c_0 - k_{off}^+ \quad (15.109)$$

and

$$\frac{dn_-}{dt} = k_{on}^- c_0 - k_{off}^-. \quad (15.110)$$

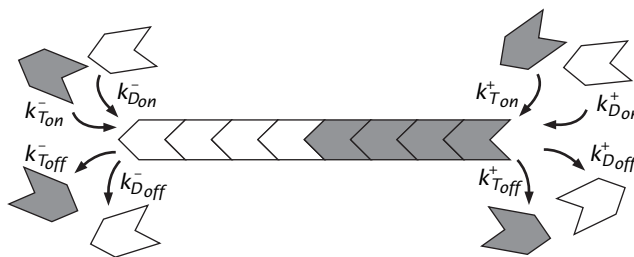
The growth rate as a function of monomer concentration is shown in Figure 15.31 and reveals that when one end grows the other suffers the same fate; this will always be the case when the concentration of monomers in solution is above c^* . This model is a reasonably accurate description of the behavior of simple polymers, such as bacterial flagellin. However, it falls short of being able to describe the entire repertoire of cytoskeletal dynamics for nucleotide hydrolyzing polymers, such as actin and microtubules. For these remarkable polymers, it is possible for one end to grow while the other is shrinking, a feature that can lead to the phenomenon of treadmilling.

15.4.3 Nucleotide Hydrolysis and Cytoskeletal Polymerization

ATP Hydrolysis Sculpts the Molecular Interface Resulting in Distinct Rates at the Ends of Cytoskeletal Filaments

The full beauty and complexity of cytoskeletal polymerization is tied to the fact that the protein monomers interact with nucleotides and, indeed, can catalyze nucleotide hydrolysis. For example, actin monomers can bind either ATP or ADP, while in the case of tubulin, they bind either GTP or GDP. The significance of this fact is that these cytoskeletal polymers behave as ATPases and by virtue of the coupling of polymerization to ATP (or GTP) hydrolysis, they can undergo

Figure 15.32 Cytoskeletal filaments with a distinction between ATP- and ADP-bound monomers. ATP-bound monomers are shaded dark and ADP-bound monomers are light. The addition of nucleotide hydrolysis to the model requires that four distinct rate constants be considered for each of the two ends of the filament.



conformational changes which alter the molecular interface between adjacent monomers and, hence, adjust the rates of binding and unbinding. The full complexity of the polymerization process was shown in Figure 15.22. For our present purposes, the key point of these observations is that there are different on and off rates for ATP-bound and ADP-bound monomers at each end of the structurally polarized actin filaments. This effect is represented schematically in Figure 15.32.

The rate equations describing this situation can be substantially simplified if we assume that on the barbed ends, only ATP-bound monomers are coming on and off, while on the pointed ends, only ADP-bound monomers are exchanged between the filament and the reservoir. In this situation, the rate equations have an identical form to those presented in eqns 15.109 and 15.110. The difference is that in this case the restriction on the ratio of the rates embodied in eqn 15.108 is no longer present. The resulting growth rates on the two ends as a function of concentration are shown in Figure 15.33.

These growth rates have a novel property relative to the other models in the hierarchy of models we have considered, namely, they can undergo the process of treadmilling. In treadmilling, one end grows while the other end shrinks. As shown in Figure 15.33, for a certain critical concentration c_{TM} the barbed end can be growing at the same rate that the pointed end is shrinking, a condition represented mathematically as

$$\frac{dn_+}{dt} = -\frac{dn_-}{dt}. \quad (15.111)$$

This condition can be written directly in terms of the rates as

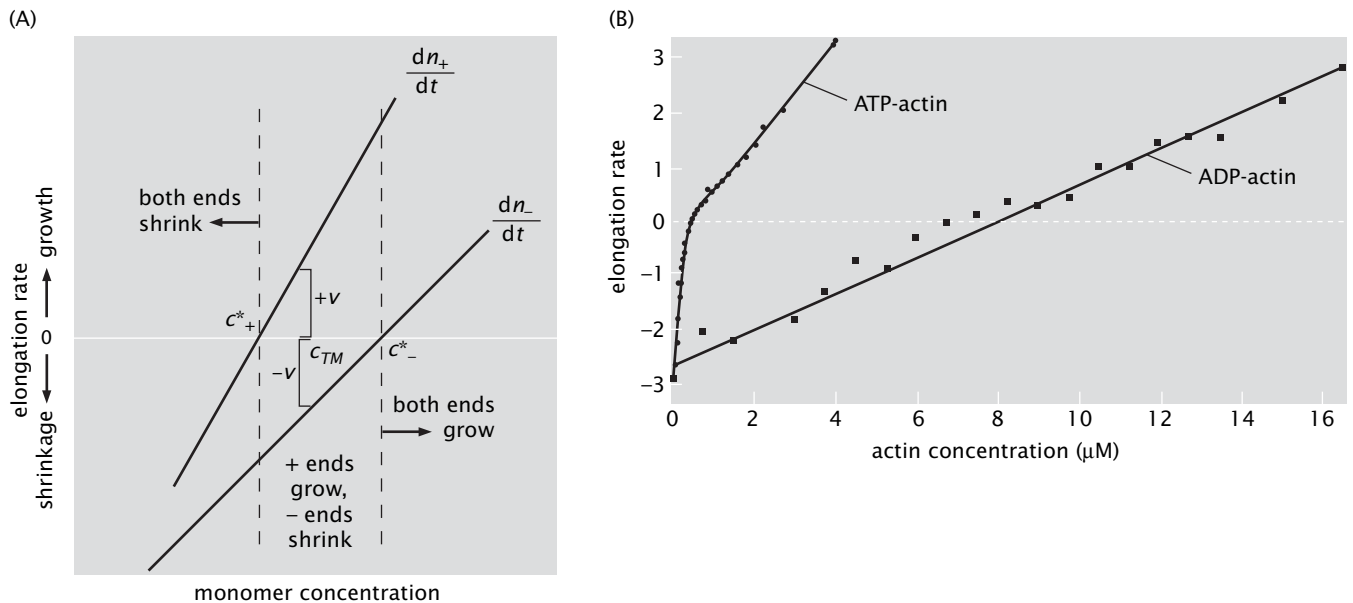
$$k_{on}^+ c_{TM} - k_{off}^+ = -k_{on}^- c_{TM} + k_{off}^-. \quad (15.112)$$

Solving this equation for c_{TM} results in the condition

$$c_{TM} = \frac{k_{off}^+ + k_{off}^-}{k_{on}^+ + k_{on}^-}, \quad (15.113)$$

which tells us how the treadmilling concentration depends upon the on and off rates on the two ends of the model polymer.

These ideas serve as the basis for thinking about the observed dynamical behavior of microtubules. In particular, under the right circumstances, it is possible to observe microtubules that are simultaneously growing on one end while shrinking at the other with the result that particular points within the microtubule lattice are fixed with respect to the absolute coordinate system of the cell. An example of this behavior is shown in Figure 15.34.



15.4.4 Dynamic Instability: A Toy Model of the Cap

One of the most intriguing features of microtubule dynamics is the existence of an effect known as “dynamic instability.” The basic observation is that an individual microtubule can undergo repeated cycles of growth and shrinkage, even when its chemical environment remains essentially constant. Similarly, a population of microtubules in the same test tube or cell will typically include some individuals that are growing and some individuals that are shrinking at any given instant in time. If the length of a single microtubule is measured as a function of time, the resulting graph is a series of sawtooths such as are shown in Figure 15.35. That is, the dynamics of microtubule growth is punctuated by occasional catastrophes, where the filament shrinks, and rescues, where it begins to grow again. Dynamic instability has also been observed in the bacterial actin-like filament ParM. It has been argued that dynamic instability provides a mechanism for repeated attempts for cytoskeletal filaments to explore the large cytoplasmic space and find their targets during chromosome segregation and other spatially complex processes.

A Toy Model of Dynamic Instability Assumes That Catastrophe Occurs When Hydrolyzed Nucleotides Are Present at the Growth Front

As a first step towards understanding the dynamics of catastrophes, we consider a simple toy model of the unhydrolyzed cap. Our picture of the growing filament is that it presents a cap of GTP (or ATP) bound monomers such as is shown in Figure 15.36. The length of this cap is determined by a competition between the rate at which monomers are being added to the end of the growing filament and the rate at which hydrolysis occurs within the filament. Within this model, catastrophe is hypothesized to occur when the cap length shrinks to zero.

To see how this might work, we begin with a deterministic model in which it is assumed that the only subunit within the filament that is able to perform nucleotide hydrolysis is the one found at the interface between the cap and the rest of the filament. Furthermore, for

Figure 15.33 Growth rates on the two ends as a function of concentration for the case in which there is nucleotide hydrolysis. (A) The two curves show the growth rates on the two ends of a microtubule as a function of the concentration of monomers. The upper curve shows the faster growth rate on the plus end. At the critical concentration, c_{TM} , the growth rate on the plus end is equal to the shrinkage rate on the minus end, resulting in treadmilling. (B) Growth rate as a function of actin concentration for ATP-actin (left) and ADP-actin (right). ADP-actin behaves as predicted by the model described in the text displaying a critical concentration at about $8 \mu\text{M}$. For ATP-actin, the growth rate above the critical concentration is a linear function of actin concentration as expected; however, the curve becomes nonlinear at lower concentrations. This is because ATP hydrolysis is accelerated by polymerization so the disassembling species is actually ADP actin. In other words, the ATP cap (see below Figure 15.36) has vanished on the shrinking filaments. (B, adapted from M. F. Carlier et al., *J. Biol. Chem.*, 259:9983, 1984.)

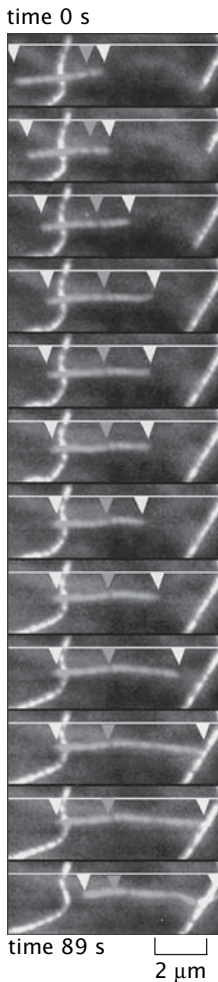


Figure 15.34 Microtubule treadmilling. Individual microtubules have been observed to undergo treadmilling inside living cells. The fluorescently labeled microtubule looks as though it is sliding from left to right. However, as indicated by the middle arrow which points to a fixed point within the microtubule, in fact one end (the minus end, on the left) is shortening and the other (the plus end, on the right) is elongating. (Adapted from C. M. Waterman-Storer and E. D. Salmon, *J. Cell Biol.*, 139:417, 1997.)

this vulnerable subunit, the rate of nucleotide hydrolysis (conversion of GTP to GDP or of ATP to ADP) is characterized by a lifetime τ . This deterministic picture implies that the position of the interface moves along the filament with a characteristic velocity a/τ . Also note that the pointed ends have rate constants characterized by ADP-bound filament ends while the growing barbed ends are characterized by the ATP rate constants. A more sophisticated and physically realistic scenario, where hydrolysis can happen at any point along the cap, would provide a more complete picture of the cap dynamics.

Within this simple model, the onset of catastrophe occurs when and if the hydrolysis “front” catches up with the growing tip on the barbed end. One physical mechanism that could lead to this effect would be a slowing down of the growing tip due to depletion of the reservoir of available monomers. Recall that our picture is that the leading edge of the filament has a velocity V and that the hydrolysis takes place at a rate $1/\tau$. Within this model, the critical condition for a catastrophe is that the velocity of the hydrolysis front equals that of the growing tip and given by

$$\underbrace{\frac{dx_{tip}}{dt}}_{\text{growth rate of leading edge}} = \underbrace{\frac{a}{\tau}}_{\text{speed of hydrolysis front}}. \quad (15.114)$$

This equation says that in the time it takes for the next monomer to be added to the growing tip the monomer at the tip will have time to hydrolyze its trinucleotide, where we have made the simplifying assumption that the cap is only one monomer in width. The critical condition written mathematically above really sets the bound since it is only when the hydrolysis front is moving faster than the growing tip that we are guaranteed that the front will catch up with the tip and induce a catastrophe.

The physical picture of the catastrophe, then, is that the catastrophe starts once the hydrolysis front catches the leading edge, because at that point the GTP (or ATP) growth rates are superseded by their GDP (or ADP) counterparts. Said differently, the off rate dominates for the GDP monomers, whereas the on rate dominates for the GTP monomers. This model predicts a very specific dependence of the catastrophe rate on the concentration of monomers available for growth. To see this, we turn to the mathematical implementation of the model.

The growth of the tip is essentially described by eqn 15.88 with the observation that $dx_{tip}/dt = adn/dt$, and results in

$$\frac{dx_{tip}}{dt} = a \left[k_{on} \left(c_0 - \frac{x_{tip}M}{Va} \right) - k_{off} \right], \quad (15.115)$$

where M is the number of growing filaments. Note that x_{tip}/a tells us the number of monomers per filament which when multiplied by M gives the total number of monomers tied up in filaments. The solution to this equation proceeds exactly as did the solution to eqn 15.88 and is plotted in Figure 15.37, and given by

$$x_{tip}(t) = \frac{aV}{Mk_{on}} (k_{on}c_0 - k_{off})(1 - e^{-Mk_{on}t/V}). \quad (15.116)$$

In this toy model, a catastrophe occurs when the speed of the tip drops just below the hydrolysis speed. This happens at a certain critical length of the cap x_{tip}^{crit} where, because of depletion of the reservoir of soluble monomers, the tip growth rate has slowed sufficiently to match the

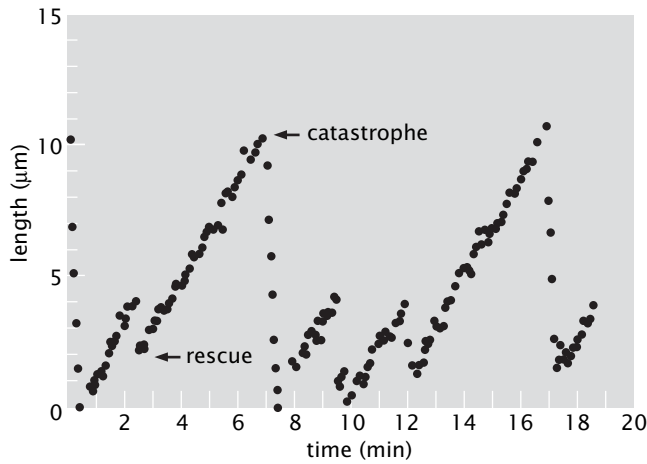


Figure 15.35 Natural history of the length variation for a single microtubule over time. A $10\ \mu\text{m}$ long microtubule was imaged in the microscope and its length measured roughly 10 times per minute. Almost immediately upon the beginning of this observation, the microtubule underwent a catastrophe and shrank rapidly to near zero length. It then underwent a rescue and began to grow again. Over the subsequent 20 min the cycle repeated 5 more times, with the lengths of the growing and shrinking phases varying randomly. Microtubule growth took place at a nearly constant rate for all cycles, and shrinkage also took place at a constant, though faster rate. (Adapted from D. K. Fygenson et al., *Phys. Rev.*, E50:1579, 1994.)

hydrolysis speed. This is characterized by the condition

$$a \left[k_{on} \left(c_0 - \frac{x_{tip} M}{Va} \right) - k_{off} \right] = \frac{a}{\tau}. \quad (15.117)$$

This equation can be solved for the critical length which is given by

$$x_{tip}^{crit} = \frac{Va}{Mk_{on}} \left(k_{on} c_0 - k_{off} - \frac{1}{\tau} \right). \quad (15.118)$$

In addition to the critical length, we are also interested in the waiting time, t_{crit} , before a catastrophe. To explore this question, we use eqn 15.116 to write $x_{tip}(t_{crit})$ and set this equal to the result in eqn 15.118 to obtain

$$e^{Mk_{on}t_{crit}/V} = \tau(k_{on}c_0 - k_{off}). \quad (15.119)$$

This equation can be solved for the time until a catastrophe as

$$t_{crit} \simeq \frac{V}{Mk_{on}} \ln(\tau k_{on}c_0), \quad (15.120)$$

where we have made the approximation $k_{off} \ll k_{on}c_0$, which is equivalent to stating that the rate of addition of new monomers to the cap will be much higher than the rate at which monomers are removed. We can now plot the catastrophe rate $1/t_{crit}$ (Figure 15.38(A)).

One of the shortcomings of this model is that it predicts that once the monomers are depleted, all microtubules will suffer catastrophes at essentially the same time. However, this prediction is clearly at odds with experimental observations on microtubule dynamics, where some microtubules can be seen to shrink (that is, undergo catastrophe) while others are growing nearby inside a living cell. This merely demonstrates that our toy model, while a useful starting point, is inadequate to describe the full complexity of microtubule behavior. A first step toward

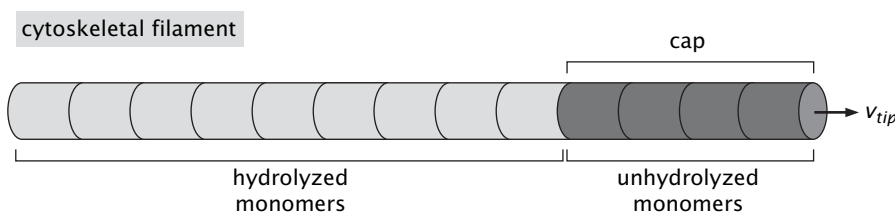


Figure 15.36 A filament presenting a cap of GDP (or ATP) bound monomers. The monomers in the cap have not yet performed nucleotide hydrolysis.

Figure 15.37 Position of the tip of a growing filament as a function of time. The instantaneous velocity of the tip (that is, the growth rate) is given as the slope of this curve. As a result of monomer depletion, the tip growth rate slows down over time.

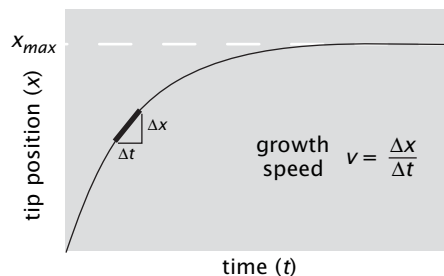
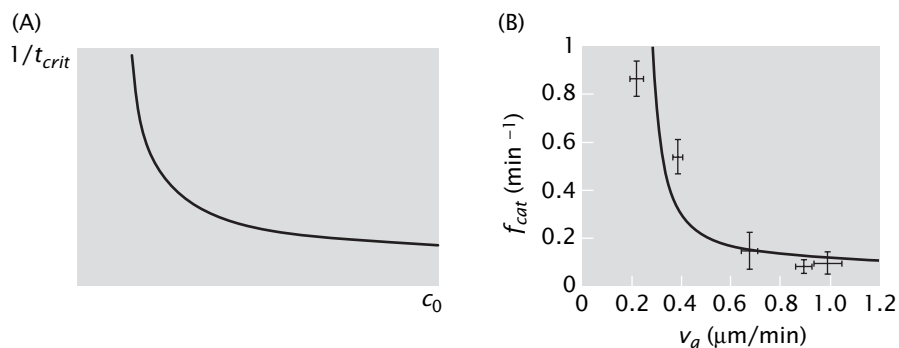


Figure 15.38 Catastrophe rate for filaments undergoing dynamic instability. (A) Catastrophe rate as a function of the monomer concentration as predicted by the toy model of cap dynamics. (B) Measured catastrophe rate as a function of the growth velocity (which is linearly related to the monomer concentration). (B, adapted from H. Flyvbjerg et al., *Phys. Rev. E* 54:5538, 1996.)



improving the accuracy of the model is to imagine that hydrolysis can occur not only at the hydrolyzed–nonhydrolyzed interface shown in Figure 15.36, but also at other positions within the cap. That is, by chance the hydrolysis event can occur very near to the end of the cap and a hydrolysis “front” can propagate away from this hydrolysis site in both the plus and minus directions. This conceptual scheme is illustrated in Figure 15.21(D). The results of this more sophisticated model for the catastrophe rate are shown in Figure 15.38(B). Here, instead of plotting the rate of catastrophes as a function of the monomer concentration, the experimental results are shown as a function of the growth velocity since this velocity is itself a linear function of the concentration. Though an analysis of this model is beyond the scope of this chapter, the reader is encouraged to examine Flyvbjerg et al. (1996) to see how the details play out. Another consideration that can lead to different behaviors for two individual microtubules in the same chemical environment is the fact that the average velocities associated with both tip growth and nucleotide hydrolysis are subject to the kinds of fluctuations illustrated in Figure 15.25. Thus, a particular microtubule may lose its cap simply by bad luck even when overall conditions favor net polymerization. This stochastic consideration almost certainly applies to microtubule dynamics in living cells.

15.5 SUMMARY AND CONCLUSIONS

Cells are a bustling environment in which huge numbers of chemical reactions are taking place constantly. As a result, an important part of the modeling toolkit for thinking about the behavior of cells are tools that model reaction dynamics. The main goal of this chapter has been the development of one particularly important paradigm for modeling chemical reactions, namely, the theory of rate equations. These equations characterize the time variation of concentrations of reactants and products in a chemical reaction of interest.

15.6 PROBLEMS

15.1 Census of cytoskeletal proteins in fission yeast

Consider the measurements shown in Figure 15.4 where global and local concentrations of various cytoskeletal proteins in fission yeast cells were determined using fluorescence microscopy. Here we make use of the measured concentrations, reported in Table 1 of Wu and Pollard (2005), to make estimates for the fission yeast cytoskeleton.

(a) Estimate the volume of a fission yeast cell and use this in turn to estimate the mean spacing between actin monomers, between capping proteins, and between formins.

(b) About half of the actin monomers in the yeast cell are in filamentous form at any given time. Given the dissociation constant for capping proteins, $K_d = 1$ nM, estimate the average length of actin filaments, assuming one capping protein per filament. Compare your estimate to the typical value which is on the order of 100 monomers per filament.

15.2 Dynamics of isomerization reactions In eqn 15.22 we described the kinetics of an isomerization reaction. Here we do the math and explore a couple of examples of this reaction.

(a) Work out the solution for the concentrations of both species and make plots of $c_A(t)$, $c_B(t)$, and their sum. Assume that initially there are only molecules of species A present, at concentration c_0 .

(b) Apply the results of (a) to the decay of 13-*cis*-retinal to all-*trans*-retinal, as was illustrated in Figure 15.8. The half-life of this reaction is $\tau = 2$ s.

(c) At a very different time scale these same ideas apply to radiometric dating. A celebrated example is the decay of potassium to argon with a half-life of 1.26 billion years. Plot the amount of argon as a function of time, assuming initially only potassium is present.

15.3 Rate equations for interconversion Consider the reversible reaction



In this case, the rate equations of interest can be written as

$$\frac{dc_A}{dt} = -k_+c_A + k_-c_B \quad (15.122)$$

and

$$\frac{dc_B}{dt} = -\frac{dc_A}{dt}, \quad (15.123)$$

with the constraint of mass conservation of the form given in eqn 15.21. In this case, the long time behavior is nonzero concentrations of both A and B.

(a) Solve these equations for $c_A(t)$ and $c_B(t)$ assuming only the molecular species A is present at time $t = 0$. Make plots of the solutions and demonstrate that the long time behavior is dictated by the ratio k_+/k_- .

(b) Using the current recording for a single sodium ion channel shown in Figure 7.2(A), estimate the opening and the closing rate of the channel. Use the result from (a) to plot the probability that the channel is open and the probability it is closed as a function of time. Assume the channel to be closed initially.

15.4 Lattice model for bimolecular reactions Fill in all of the details in the derivation of eqn 15.32 for the bimolecular reaction rate, given in Section 15.2.4.

15.5 Michaelis–Menten vs exact kinetics Write the full set of rate equations for the reaction described by the Michaelis–Menten kinetic model. Introduce dimensionless variable by measuring time in units of $k_- + r$, concentrations in units of $K_m = (k_- + r)/k_+$ and define $\varepsilon = r/(r + k_-)$.

(a) Solve these equations numerically and reproduce Figure 15.16(A).

(b) Make a plot of $d[P]/dt$ vs $[S]$ using both the Michaelis–Menten form and the exact solution for the following choices of parameters: (i) $[S]_0 = 100$, $[E]_0 = 1$, $\varepsilon = 0.1$, and (ii) $[S]_0 = 1$, $[E]_0 = 1$, $\varepsilon = 1$. What conclusion do you draw about the validity of the Michaelis–Menten form?

15.6 Toy model of the cell cycle

(a) Write a simple system of differential equations to model the cyclin and cyclin-dependent kinase activity oscillations. Assume that cyclin is produced at a constant rate and that its degradation rate depends on the concentration of cyclin-dependent kinase. Similarly, assume that the production rate of cyclin-dependent kinase depends on the concentration of cyclin and that it has a constant degradation rate.

(b) Assume a linear dependence of the degradation rate of cyclin, and the production rate of cyclin-dependent kinase, on the concentration of cyclin-dependent kinase and cyclin, respectively. Solve the system of equations for different initial conditions and rates. Comment on the conditions under which oscillations are obtained.

15.7 Microtubule dynamics and dynamic instability

In this problem we consider a phenomenological model for steady state microtubule dynamics that was introduced by Dogterom and Leibler (1993). Note that there is a more interesting class of models that include GTP hydrolysis explicitly (see Flyvbjerg et al. (1996)). The goal of such models is to respond to data such as those in Figure 15.35. This figure shows a record of the length of a single microtubule as a function of time and reveals the series of “catastrophes” and “rescues” as the polymer changes its length.

(a) Deduce the following equations for the probability distributions $p_+(n, t)$ and $p_-(n, t)$ which give the probability of finding a microtubule:

$$\frac{\partial p_+}{\partial t} = -f_+p_+ + f_-p_- - v_+ \frac{\partial p_+}{\partial z} \quad (15.124)$$

$$\frac{\partial p_-}{\partial t} = +f_+p_+ - f_-p_- + v_+ \frac{\partial p_-}{\partial z} \quad (15.125)$$

Write a master equation for $p_+(n, t)$ and $p_-(n, t)$ by noting that there are four processes that can change the probability at each instant. Consider the + case: (i) the $n - 1$ polymer can grow and become an n polymer, characterized by a rate v_+ , (ii) the n polymer can grow and become an $n + 1$ polymer, also characterized by a rate v_+ , (iii) the $n + 1$ polymer can switch from growing to shrinking with a rate f_{+-} and (iv) the $n -$ polymer can switch from shrinking

to growing with a rate f_{-+} . If you account for all four of these possibilities you will have the correct master equation. Use a Taylor expansion on factors like $p_+(n-1, t) - p_+(n, t)$ to obtain eqns 15.124 and 15.125.

(b) Solve these equations for $p_{\pm}(n)$ in the steady state (that is, $\partial p_{\pm}(n, t)/\partial t = 0$). Show that in the steady state the probabilities $p_{\pm}(n)$ decay exponentially with constant

$$\sigma = \frac{v_+ f_{-+} - v_- f_{+-}}{v_+ v_-}. \quad (15.126)$$

(c) Use Figure 15.35 to estimate the parameters v_+, v_-, f_{+-}, f_{-+} , and then find the average length of the polymers which is *predicted* by this simple model. To find the average length you will need to sum over all lengths with their appropriate probability. The slopes of the growth and decay regions tell you about the on and off rates, and the durations of the growth and decay periods tell you something about the parameters f_{+-} and f_{-+} . Note that by fitting the dynamical data, you are deducing/predicting something about the distribution of lengths.

15.7 FURTHER READING

Segel, LA (1984) Modeling Dynamic Phenomena in Molecular and Cell Biology, Cambridge University Press. Segel's book provides a wonderful discussion of many of the topics covered in the present chapter.

Michaelis, L, & Menten, ML (1913) Kinetics of invertase action, *Z. Biochem.* **49**, 333. This classic paper outlines the theoretical framework used by biochemists to study the kinetics of enzymatic catalysis.

Crane, HR (1950) Principles and problems of biological growth, *Sci. Monthly* **70**, 376. This fascinating article shows how the assembly of objects having no particular symmetry favors helical geometries.

Abraham, VC, Krishnamurthi, V, Taylor, DL, & Lanni, F (1999) The actin-based nanomachine at the leading edge of migrating cells, *Biophys. J.*, **77**, 1721. This paper, like that of Wu and Pollard (2005), presents a census of actin, in this case at the leading edge of motile cells.

Oosawa, F, & Asakura, S (1975) Thermodynamics of the Polymerization of Protein, Academic Press. This classic book is full of interesting pictures and discussion of the polymerization problem.

Amos, LA, & Amos WB, (1991) Molecules of the Cytoskeleton, The Guilford Press. This book is full of interesting insights into the cytoskeleton.

Hill, TL, & Kirschner, MW (1982) Bioenergetics and kinetics of microtubules and actin filament assembly-disassembly, *Int. Rev. Cytol.* **78**, 1. This comprehensive paper lays out the theoretical basis for kinetics and thermodynamics of protein polymerization for every possible case; with and without structural polarity, with and without nucleotide hydrolysis, in the presence of capping proteins and in the presence of loads or barriers.

Flyvbjerg, H, Holy, TE, & Leibler, S (1996) Microtubule dynamics: Caps, catastrophes, and coupled hydrolysis, *Phys. Rev.* **E54**, 5538. This interesting paper shows how to go beyond the simple model of the cap described in the chapter to include stochastic dissolution of the cap by hydrolysis.

Caplow, M, & Shanks, J (1996) Evidence that a single monolayer tubulin-GTP cap is both necessary and sufficient to stabilize microtubules, *Mol. Biol. Cell* **7**, 663. This paper describes experiments on the nature of the GTP cap in microtubules.

15.8 REFERENCES

Alberts, B, Johnson, A, Lewis, J, et al. (2008) Molecular Biology of the Cell, 5th ed. Garland Science.

Brown, AJ (1902) Enzyme action, *J. Chem. Soc. Trans.*, **81**, 373.

Burlacu, S, Janmey, PA, & Borejdo, J (1992) Distribution of actin filament lengths measured by fluorescence microscopy, *Am. J. Physiol.* **262**, C569.

Campbell, CS, & Mullins, RD (2007) *In vivo* visualization of type II plasmid segregation: bacterial actin filaments pushing plasmids, *J. Cell Biol.*, **179**, 1059.

Carlier, MF, Pantaloni, D, & Korn, ED (1984) Evidence for an ATP cap at the ends of actin filaments and its regulation of the F-actin steady state, *J Biol. Chem.* **259**, 9983.

Dogterom, M, & Leibler, S (1993) Physical aspects of the growth and regulation of microtubule structures, *Phys. Rev. Lett.* **70**, 1347.

Fygenson, DK, Braun, E, & Libchaber, A (1994) Phase diagram of microtubules, *Phys. Rev.* **E50**, 1579.

Garner, EC, Campbell, CS, & Mullins, RD (2004) Dynamic instability in a DNA-segregating prokaryotic actin homolog, *Science* **306**, 1021.

Hermone, A, & Kuczera, K (1998) Free-energy simulations of the retinal *cis* \rightarrow *trans* isomerization in bacteriorhodopsin, *Biochem.* **37**, 2843.

Iino, T (1974) Assembly of *Salmonella* flagellin *in vitro* and *in vivo*, *J. Supramol. Struct.* **2**, 372.

Keller, BU, Hartshorne, RP, Talvenheimo, JA, Catterall, WA, & Montal, M (1986) Sodium channels in planar lipid bilayers. Channel gating kinetics of purified sodium channels modified by batrachotoxin, *J. Gen. Physiol.* **88**, 1.

Ouellete, L, Laidler, KJ, & Morales, MF (1952) Molecular kinetics of muscle adenosine triphosphatase, *Arch. Biochem. Biophys.* **39**, 37.

Pollard, TD (1986) Rate constants for the reactions of ATP- and ADP-actin with the ends of actin filaments, *Cell Biol.* **103**, 2747.

Waterman-Storer, CM, & Salmon, ED (1997) Actomyosin-based retrograde flow of microtubules in the lamella of migrating epithelial cells influences microtubule dynamic instability and turnover and is associated with microtubule breakage and treadmilling, *J. Cell Biol.* **139**, 417.

Welch, MD, Rosenblatt, J, Skoble, J, Portnoy, DA, & Mitchison, TJ (1998) Interaction of human Arp2/3 complex and the *Listeria monocytogenes* ActA protein in actin filament nucleation, *Science*, **281**, 105.

Wu, J-Q, & Pollard, TD (2005) Counting cytokinesis proteins globally and locally in fission yeast, *Science* **310**, 310. This paper illustrates the strategy of using fluorescence microscopy for taking the census of a cell.